Research Square

Preprints are preliminary reports that have not undergone peer review.
They should not be considered conclusive, used to inform clinical practice,
or referenced by the media as validated information.

Properties and Statistical Inference for the Standard Gram--Charlier Type A Distribution and Its Exponentiated Version

Sthitadhi Das

sthdas999@gmail.com

Brainware University https://orcid.org/0009-0001-2484-9530

Subhrajit Saha

Visva-Bharati University

Research Article

Keywords: Gram--Charlier expansion, cumulants, Hermite polynomials, characteristic function, moment generating function, skewness, kurtosis

Posted Date: July 7th, 2026

DOI: https://doi.org/10.21203/rs.3.rs-10245873/v1

License: This work is licensed under a Creative Commons Attribution 4.0 International License.
Read Full License

Additional Declarations: The authors declare no competing interests.

Properties and Statistical Inference for the Standard Gram–Charlier Type A Distribution and Its Exponentiated Version

Sthitadhi Das [1,*], Subhrajit Saha[2]
[1] Department of Mathematics, Brainware University, India
[2] Department of Statistics, Visva-Bharati University, India
[*]Corresponding author: sthdas999@gmail.com

Abstract

The purpose of the present paper is to offer basic results on the standardization of Gram–Charlier Type A (GC(A)) distribution; indeed, we derive the normalization conditions and the characteristic and cumulant-generating function of the standardized distribution, the link between moments and cumulants of it, the first few moments of the standardized distribution and relation between skewness, kurtosis and higher order cumulants, and, finally we comment on some defect of the truncated expansion, mainly the non-negativity property and whether GC(A) expansion can be a pdf.

Keywords: Gram–Charlier expansion; cumulants; Hermite polynomials; characteristic function; moment generating function; skewness; kurtosis.
Mathematics Subject Classification (2020): 62E10 (primary); 60E10, 62E15 (secondary).

1 Introduction

Historically, an approach that may be considered one of the first that was utilized to develop approximations of probability distributions is by using a series expansion of mutually orthogonal polynomials. Representation of distribution function in form of series of orthogonal polynomials provides the representation for non-Gaussian distribution, in which non-Gaussianness is given in terms of basis functions as polynomials. An important attempt to use the polynomial expansion of probability functions was done by Gram [5] and Charlier [2, 3]. The former attempted to represent any statistical distribution in a form of power series expansion in terms of Hermite polynomials. Subsequently this developed into one of the significant, areas in theory on the asymptotic properties of statistical distributions and the methods in the higher-order statistics.

One of the commonly used orthogonal expansions is the Gram-Charlier Type A (GC(A)) series which expand upon the standard normal distribution to add correction terms based

on higher order cumulants. Therefore, such expansions allow for deviations from normality to be taken into account, as well as skewedness and excess kurtosis. Such expansion of densities into basis sets is amenable to analytical methods since the probabilist's Hermite polynomials serve as a basis set with the 'natural' orthogonality given by the Gaussian weighting function. Classic accounts on the theory of cumulants and the role and implications of Hermite expansions can be found in, for example, Kendall and Stuart [6] and Cramér [4].

The Edgeworth expansion, similar to the Gram-Charlier expansion, plays a role in asymptotic theory [1]. For sums of independent variables, extensions of Edgeworth expansion were developed within the context of an limiting procedure whereas Gram-Charlier is regarded as density at some order of cumulants. While both of them represent the approximation beyond normal approximation, they are applicable in very different settings and the convergences are very different.

Although Gram-Charlier Type A distribution has been an important part of theoretical statistics, it is mostly dealt with from the asymptotic viewpoint: a limited number of authors tried to work out some properties of the distribution after its standardization as a whole. Characteristic function, cumulant generating function, and moment-cumulants are derived separately from place to place. What most deserves criticism of the truncated expansion is the fact that the negative value comes up for the tails of the distribution, therefore impairing the representability of the distribution, that is, non-negativity, is typically neither mentioned nor cursorily discussed.

This paper is devoted to the exhaustive and formal analysis of the standardized Gram–Charlier Type A distribution. This article covers the derivation of the normalized form of the distribution as well as the derivation of its characteristic and cumulant generating function. Furthermore the low-order raw and central moments of the distribution were derived and an analysis was presented showing how skewness and kurtosis act as functions of higher order cumulants. Our derivations reflect the robustness of the Gram–Charlier Type A distribution and of its truncations to a finite order for describing departures from the normal law.

This paper represents a starting point in the construction of a theoretic structure accurate enough to analyze problems which is purely analytic and that may be solved also via computers, using the techniques related to the approximation by cumulants. A second,original contribution of this work is to compare the structure of the Exponentiated Gram–Charlier Type A distribution with that of the Exponentiated Zeghdoudi distribution (the modified zeghdoudi distribution, in the sense of [7], structure of which will be analyzed as well). This, together with the higher order cumulants considered, allows us to detect both similarities and differences between the two models and growth of their moments.

While for the exp{GC(A)} distribution, moments grow like $e^{k^2/2}$ (growth quadratic-exponential), EZ distribution follows an (infinite) exponential-polynomial moment growth pattern of gamma-like shape; providing in this way, an adequate framework to study Gram–Charlier perturbations and moment growth patterns.

As far as we are concerned, this is the first comparative study of moment growth between cumulant-based exponentiated models and gamma-mixture-based exponentiated models.

2 The Standard Gram–Charlier Type A Distribution: Structure and Properties

This section develops the analytical structure of the standardized Gram–Charlier Type A (GC(A)) distribution, including its definition, normalization, characteristic function, cumulant generating function, moment structure, and implications for transformed sample moments.

2.1 Definition and Standardization

Let $\phi(x)$ denote the standard normal density $\phi(x) = \dfrac{1}{\sqrt{2\pi}} e^{-x^2/2}$. The standardized Gram–Charlier Type A expansion is defined as

$$f(x) = \phi(x) \left[1 + \sum_{r=3}^{\infty} \frac{\kappa_r}{r!} H_r(x) \right], \tag{2.1}$$

where κ_r denotes the r-th cumulant and $H_r(x)$ are the probabilists' Hermite polynomials defined by

$$H_r(x) = (-1)^r e^{x^2/2} \frac{d^r}{dx^r} e^{-x^2/2}. \tag{2.2}$$

For standardization purpose, we set $\kappa_1 = 0,\ \kappa_2 = 1$. Truncating the expansion at fourth order yields

$$f(x) = \phi(x) \left[1 + \frac{\kappa_3}{6} H_3(x) + \frac{\kappa_4}{24} H_4(x) \right], \tag{2.3}$$

where $H_3(x) = x^3 - 3x,\ H_4(x) = x^4 - 6x^2 + 3$. Thus,

$$f(x) = \phi(x) \left[1 + \frac{\kappa_3}{6} (x^3 - 3x) + \frac{\kappa_4}{24} (x^4 - 6x^2 + 3) \right]. \tag{2.4}$$

2.2 Normalization

Using the orthogonality property $\displaystyle\int_{-\infty}^{\infty} H_r(x)\phi(x)\,dx = 0 \quad (r \geq 1)$, we obtain $\displaystyle\int_{-\infty}^{\infty} f(x)\,dx = 1$. Hence, any finite truncation preserves total probability mass equal to one, although non-negativity is not guaranteed (see Section 2.8).

2.3 Characteristic Function

The characteristic function is $\varphi(t) = E(e^{itX})$. Using $\displaystyle\int_{-\infty}^{\infty} e^{itx} H_r(x)\phi(x)\,dx = (it)^r e^{-t^2/2}$, we obtain

$$\varphi(t) = e^{-t^2/2} \left[1 + \sum_{r=3}^{\infty} \frac{\kappa_r}{r!} (it)^r \right]. \tag{2.5}$$

Up to fourth order, $\varphi(\cdot)$ is approximated as

$$\varphi(t) = e^{-t^2/2}\left[1 + \frac{\kappa_3}{6}(it)^3 + \frac{\kappa_4}{24}(it)^4\right]. \tag{2.6}$$

2.4 Cumulant Generating Function

The cumulant generating function is $K(t) = \log \varphi(-it)$. Since $\varphi(-it) = e^{t^2/2}\left[1 + \sum_{r=3}^{\infty} \frac{\kappa_r}{r!} t^r\right]$, a logarithmic expansion gives

$$K(t) = \frac{t^2}{2} + \sum_{r=3}^{\infty} \frac{\kappa_r}{r!} t^r + O(\kappa^2). \tag{2.7}$$

Thus the distribution preserves the prescribed cumulant structure: $\kappa_1 = 0,\ \kappa_2 = 1,\ \kappa_3, \kappa_4, \ldots$

2.5 Moment Structure

2.5.1 Raw Moments

Using standard normal moments $E_\phi(X^2) = 1,\ E_\phi(X^4) = 3,\ E_\phi(X^6) = 15$, we obtain

$$\begin{aligned}
E(X^3) &= \kappa_3, \\
E(X^4) &= 3 + \kappa_4, \\
E(X^5) &= 10\kappa_3, \\
E(X^6) &= 15 + 15\kappa_4 + 10\kappa_3^2.
\end{aligned}$$

2.5.2 Central Moments and Standardized Measures

Since the distribution is standardized, we have

$$\mu_1 = 0, \quad \mu_2 = 1, \quad \mu_3 = \kappa_3, \quad \mu_4 = 3 + \kappa_4.$$

Therefore, Skewness $(\gamma_1) = \kappa_3,$ Excess Kurtosis $(\gamma_2) = \kappa_4$.

2.6 The r-th Order Absolute Sample Moment under GC(A)

Let $W \sim \mathrm{GC(A)}(\kappa_3, \kappa_4, \ldots)$ be standardized and define $Y = e^W$. For a sample $W_1, \ldots, W_n$, define

$$M_{r,n} = \frac{1}{n}\sum_{i=1}^{n} |Y_i|^r = \frac{1}{n}\sum_{i=1}^{n} e^{rW_i}, \tag{2.8}$$

since $Y_i > 0$ almost surely.

2.6.1 Exact Characteristic Function

Let $Z_i = e^{rW_i}$. Then, $M_{r,n} = \frac{1}{n}\sum_{i=1}^{n} Z_i$. Therefore, the characteristic function of Z is

$$\varphi_Z(t) = \int_{-\infty}^{\infty} e^{ite^{rw}} \phi(w) \left[1 + \sum_{m\geq 3} \frac{\kappa_m}{m!} H_m(w)\right] dw. \tag{2.9}$$

By independence, we obtain $\varphi_{M_{r,n}}(t) = \left[\varphi_Z\left(\frac{t}{n}\right)\right]^n$.

2.6.2 Cumulant-Based Approximation

If $\kappa_m(Z)$ denotes the cumulants of Z, then $\kappa_m(M_{r,n}) = \frac{\kappa_m(Z)}{n^{m-1}}$.

Hence,

$$\begin{aligned}
E(M_{r,n}) &= \kappa_1(Z), \\
\mathrm{Var}(M_{r,n}) &= \frac{\kappa_2(Z)}{n}, \\
\mathrm{Skewness}(M_{r,n}) &= \frac{\kappa_3(Z)}{\sqrt{n}\,\kappa_2(Z)^{3/2}}, \\
\text{Excess Kurtosis}(M_{r,n}) &= \frac{\kappa_4(Z)}{n\,\kappa_2(Z)^2}.
\end{aligned}$$

2.6.3 Approximate Evaluation via Fourth-Order Truncation

Using the truncated expansion, we get

$$E[e^{rW}] \approx E_\phi[e^{rW}] + \frac{\kappa_3}{6} E_\phi[e^{rW} H_3(W)] + \frac{\kappa_4}{24} E_\phi[e^{rW} H_4(W)]. \tag{2.10}$$

Since $E_\phi[e^{rW}] = e^{r^2/2}$, closed-form expressions for $E(Z)$, $E(Z^2)$, and higher moments follow. For $\kappa_3 = \kappa_4 = 0$, the model reduces to the lognormal case.

2.7 Moment–Cumulant Relations

In general, $\mu_4 = \kappa_4 + 3\kappa_2^2$, $\mu_6 = \kappa_6 + 15\kappa_4\kappa_2 + 10\kappa_3^2 + 15\kappa_2^3$. With $\kappa_2 = 1$, these simplify accordingly.

2.8 Validity and Limitations

Although the truncated Gram–Charlier expansion preserves normalization and cumulant structure, the correction polynomial may dominate in the tails, potentially producing nega-

tive densities. Consequently, the expansion should be interpreted as an analytic approximation rather than a universally valid parametric distribution.

3 Exact Distribution of the Absolute r-th Order Sample Moment

Let W follow a standardized Gram–Charlier Type A (GC(A)) distribution:

$$f_W(w) = \phi(w)\left[1 + \sum_{m\geq 3} \frac{\kappa_m}{m!} H_m(w)\right]. \tag{3.1}$$

Define the transformed variable $Y = e^W$. For a random sample $W_1, \ldots, W_n$, the absolute r-th order sample moment is $M_{r,n} = \dfrac{1}{n}\sum_{i=1}^{n} |Y_i|^r = \dfrac{1}{n}\sum_{i=1}^{n} e^{rW_i}$, since $Y_i > 0$.

3.1 Density of Y

Applying the standard transformation for positive variables, the density of Y is

$$f_Y(y) = \frac{1}{y} f_W(\log y) = \frac{1}{y}\phi(\log y)\left[1 + \sum_{m\geq 3} \frac{\kappa_m}{m!} H_m(\log y)\right], \quad y > 0. \tag{3.2}$$

3.2 Distribution of the Sample Mean

Set $Z_i = e^{rW_i},\ i = 1, \ldots, n$, so that $M_{r,n} = \dfrac{1}{n}\sum_{i=1}^{n} Z_i$. Since the Z_i's are i.i.d., deriving the distribution of $M_{r,n}$ reduces to analyzing the sample mean of the Z_i.

3.3 Characteristic Function

The characteristic function of Z_i is

$$\varphi_Z(t) = E[e^{itZ}] = \int_{-\infty}^{\infty} e^{ite^{rw}} f_W(w)\, dw = \int_{-\infty}^{\infty} e^{ite^{rw}} \phi(w)\left[1 + \sum_{m\geq 3} \frac{\kappa_m}{m!} H_m(w)\right] dw. \tag{3.3}$$

The characteristic function of the sum $S_n = \sum_{i=1}^{n} Z_i$ is $\varphi_{S_n}(t) = [\varphi_Z(t)]^n$, and by the scaling property of characteristic functions, the sample moment $M_{r,n} = S_n/n$ has

$$\varphi_{M_{r,n}}(t) = \varphi_{S_n}\left(\frac{t}{n}\right) = \left[\varphi_Z\left(\frac{t}{n}\right)\right]^n. \tag{3.4}$$

3.4 Density via Fourier Inversion

The exact density of $M_{r,n}$ can be obtained using Fourier inversion:

$$f_{M_{r,n}}(x) = \frac{1}{2\pi} \int_{-\infty}^{\infty} e^{-itx} \left[\varphi_Z \left(\frac{t}{n} \right) \right]^n dt. \tag{3.5}$$

3.5 Cumulant Representation

The cumulants of Z are defined as $\kappa_m(Z) = \left. \frac{d^m}{dt^m} \log \varphi_Z(t) \right|_{t=0}$. Then the cumulants of S_n and $M_{r,n}$ satisfy $\kappa_m(S_n) = n\kappa_m(Z),\ \kappa_m(M_{r,n}) = \frac{1}{n^{m-1}} \kappa_m(Z)$, providing an alternative exact characterization of the sample moment's distribution.

3.6 Special Case: Lognormal Benchmark

When $\kappa_m = 0$ for $m \geq 3$, W is normal and $Z = e^{rW}$ is lognormal. The present GC(A) framework thus generalizes the classical sum-of-lognormals problem.

3.7 Exact Finite-Sample Characterization

In conclusion, the exact finite-sample distribution of $M_{r,n}$ is completely determined by

$$\boxed{\varphi_{M_{r,n}}(t) = \left[\int_{-\infty}^{\infty} e^{i(t/n)e^{rw}} \phi(w) \left(1 + \sum_{m \geq 3} \frac{\kappa_m}{m!} H_m(w) \right) dw \right]^n}. \tag{3.6}$$

This expression fully characterizes the theoretical law of the r-th order absolute sample moment under the GC(A) assumption.

4 The Exponentiated Gram–Charlier Type A Distribution

4.1 Definition

Let X be a standard Gram–Charlier Type A random variable with density given by (3.1). We define the **Exponentiated Gram–Charlier Type A random variable** as

$$\boxed{Y = \exp(X)}$$

and we write $Y \sim \exp\{\text{GC(A)}\}$.

4.2 Probability Density Function

Using transformation techniques, since $X = \log Y$, we obtain

$$f_Y(y) = \frac{1}{y}\phi(\log y)\left[1 + \sum_{r=3}^{\infty} \frac{\kappa_r}{r!} H_r(\log y)\right], \qquad y > 0. \tag{4.1}$$

Thus the exponentiated GC(A) distribution can be viewed as a *Gram–Charlier perturbation of the lognormal distribution.*

4.3 Raw Moments

The kth raw moment of Y is $\mathbb{E}(Y^k) = \mathbb{E}\big(e^{kX}\big) = M_X(k)$, where $M_X(t)$ denotes the moment generating function of X. Since for GC(A),

$$M_X(t) = \exp\left(\frac{t^2}{2}\right)\left[1 + \sum_{r=3}^{\infty} \frac{\kappa_r}{r!} t^r\right] \tag{4.2}$$

we obtain

$$\boxed{\mathbb{E}(Y^k) = \exp\left(\frac{k^2}{2}\right)\left[1 + \sum_{r=3}^{\infty} \frac{\kappa_r}{r!} k^r\right]} \tag{4.3}$$

Hence, all positive integer moments exist.

4.4 Absolute Moments

For any real p, $\mathbb{E}(|Y|^p) = \mathbb{E}(Y^p) = \exp\left(\frac{p^2}{2}\right)\left[1 + \sum_{r=3}^{\infty} \frac{\kappa_r}{r!} p^r\right]$, since $Y > 0$ almost surely.

4.5 Moment Generating Function

The moment generating function of Y is $M_Y(t) = \mathbb{E}\big(e^{tY}\big) = \mathbb{E}\big(e^{te^X}\big)$, which does not admit a closed-form expression in general. However, it admits the expansion

$$M_Y(t) = \sum_{k=0}^{\infty} \frac{t^k}{k!}\mathbb{E}(Y^k) = \sum_{k=0}^{\infty} \frac{t^k}{k!} \exp\left(\frac{k^2}{2}\right)\left[1 + \sum_{r=3}^{\infty} \frac{\kappa_r}{r!} k^r\right] \tag{4.4}$$

4.6 Cumulants

Let $K_X(t)$ denote the cumulant generating function of X:

$$K_X(t) = \log M_X(t) = \frac{t^2}{2} + \sum_{r=3}^{\infty} \frac{\kappa_r}{r!} t^r \tag{4.5}$$

Since $\mathbb{E}(Y^k) = M_X(k)$, the logarithm of the kth moment of Y satisfies

$$\log \mathbb{E}(Y^k) = \frac{k^2}{2} + \sum_{r=3}^{\infty} \frac{\kappa_r}{r!} k^r \tag{4.6}$$

Thus, the cumulants of $\log Y$ coincide with those of X:

$$\kappa_r(\log Y) = \kappa_r(X), \qquad r \geq 1 \tag{4.7}$$

The cumulants of Y itself can be obtained from the formal expansion

$$\log M_Y(t) = \sum_{m=1}^{\infty} \frac{\kappa_m^{(Y)}}{m!} t^m \tag{4.8}$$

where $\kappa_m^{(Y)}$ can be expressed through Bell polynomial relations applied to $\mathbb{E}(Y^k)$.

4.6.1 Remarks

The exponentiated GC(A) distribution can be viewed as a natural extension of the lognormal model, enriched by the inclusion of higher-order cumulant perturbations. In the special case where $\kappa_r = 0$ for all $r \geq 3$, the model simplifies to the standard lognormal distribution. By construction, the distribution is supported on positive values and typically exhibits right-skewness. Its tail behaviour is influenced not only by the underlying Gaussian quadratic growth but also by the additional higher-order cumulant terms, which allow for greater flexibility in capturing extreme outcomes.

4.7 Exact and Asymptotic Law of the Sample Absolute Moment

Let $Y_1, \ldots, Y_n$ be i.i.d. random variables such that $Y_i \sim \exp\{\text{GC(A)}\}$. Since $Y_i > 0$ almost surely, the pth absolute moment equals the pth raw moment. Define the sample absolute moment $\widehat{m}_{p,n} = \dfrac{1}{n}\sum_{i=1}^{n} Y_i^p, \qquad p > 0.$

The population absolute moment is given by

$$m_p = \mathbb{E}(Y^p) = \exp\left(\frac{p^2}{2}\right)\left[1 + \sum_{r=3}^{\infty} \frac{\kappa_r}{r!} p^r\right] \tag{4.9}$$

4.7.1 Exact Finite-Sample Distribution

Let $Z_i = Y_i^p$. Then $\widehat{m}_{p,n} = \dfrac{1}{n}\sum_{i=1}^{n} Z_i$, where Z_i are i.i.d. positive random variables. The moment generating function (m.g.f.) of Z_i is $M_Z(t) = \mathbb{E}\big(e^{tY^p}\big) = \sum_{k=0}^{\infty} \dfrac{t^k}{k!}\mathbb{E}(Y^{pk})$, where $\mathbb{E}(Y^{pk}) = \exp\left(\dfrac{(pk)^2}{2}\right)\left[1 + \sum_{r=3}^{\infty} \dfrac{\kappa_r}{r!}(pk)^r\right]$. Hence, the exact mgf of the scaled sample moment satisfies $M_{\widehat{m}_{p,n}}(t) = \left[M_Z\left(\dfrac{t}{n}\right)\right]^n$.

Thus, the finite-sample distribution of $\widehat{m}_{p,n}$ is completely characterized through the above **m.g.f.**. The exact mean and variance are given by $\mathbb{E}(\widehat{m}_{p,n}) = m_p$ and $\text{Var}(\widehat{m}_{p,n}) =$

$\frac{1}{n}\left(m_{2p} - m_p^2\right)$, where $m_{2p} = \exp\left(\frac{(2p)^2}{2}\right)\left[1 + \sum_{r=3}^{\infty} \frac{\kappa_r}{r!}(2p)^r\right]$.

4.7.2 Strong Law of Large Numbers

If $m_p < \infty$, then $\widehat{m}_{p,n} \xrightarrow{\text{a.s.}} m_p\,;\, n \to \infty$. Thus, the sample absolute moment is strongly consistent.

4.7.3 Asymptotic Normality

If $m_{2p} < \infty$, then by the classical Central Limit Theorem,

$$\sqrt{n}\left(\widehat{m}_{p,n} - m_p\right) \xrightarrow{d} \mathcal{N}\left(0, \sigma_p^2\right),$$

where $\sigma_p^2 = m_{2p} - m_p^2$. Equivalently, $\widehat{m}_{p,n} = m_p + \frac{\sigma_p}{\sqrt{n}} Z + o_p(n^{-1/2})$, with $Z \sim \mathcal{N}(0,1)$.

4.7.4 Delta-Method Refinement

Consider a smooth functional $g(\cdot)$. Then,

$$\sqrt{n}\left(g(\widehat{m}_{p,n}) - g(m_p)\right) \xrightarrow{d} \mathcal{N}\left(0, [g'(m_p)]^2 \sigma_p^2\right) \tag{4.10}$$

In particular, for the logarithmic absolute moment,

$$\sqrt{n}\left(\log \widehat{m}_{p,n} - \log m_p\right) \xrightarrow{d} \mathcal{N}\left(0, \frac{\sigma_p^2}{m_p^2}\right) \tag{4.11}$$

4.7.5 Asymptotic Expansion

A second-order expansion yields $\widehat{m}_{p,n} = m_p + \frac{1}{n}\sum_{i=1}^{n}\left(Y_i^p - m_p\right)$, and hence we get

$$\text{Bias}(\widehat{m}_{p,n}) = 0, \;\; \text{MSE}(\widehat{m}_{p,n}) = \frac{\sigma_p^2}{n}.$$

Higher-order corrections can be derived using cumulant expansions of Z_i.

4.7.6 Remark on Tail Influence

Since $m_{2p} = \exp\left(2p^2\right)\left[1 + \sum_{r=3}^{\infty} \frac{\kappa_r}{r!}(2p)^r\right]$, the asymptotic variance grows super-exponentially in p. Thus high-order sample absolute moments exhibit increasing instability, especially when higher-order cumulants κ_r are large.

5 Simulation Setup for GC (A)

To illustrate and validate the theoretical results for the absolute r-th order sample moment $M_{r,n}$, we conducted a series of Monte Carlo simulations. The simulation design is described below.

5.1 Random Sample Generation

Let $W \sim \text{GC(A)}(\kappa_3, \kappa_4)$ denote a standardized Gram–Charlier Type A distribution with specified skewness κ_3 and excess kurtosis κ_4. A random sample of size n is generated using the following steps:

1. Generate n independent standard normal variables $Z_i \sim \mathcal{N}(0, 1)$.
2. Construct the Gram–Charlier Type A approximation via $W_i = Z_i + \sum_{m=3}^{4} \frac{\kappa_m}{m!} H_m(Z_i)$.
3. Transform to the variable of interest: $Y_i = e^{W_i},\ i = 1, \ldots, n$.

5.2 Absolute r-th Order Sample Moment

For each simulated sample $\{Y_1, \ldots, Y_n\}$, the absolute r-th order sample moment is computed as $M_{r,n} = \frac{1}{n} \sum_{i=1}^{n} |Y_i|^r = \frac{1}{n} \sum_{i=1}^{n} Y_i^r$.

5.3 Parameter Settings

The simulations were conducted over a range of parameter settings to examine how skewness, kurtosis, sample size, and the order r influence the results. Specifically, sample sizes of $n = 20, 50, 100$, and 500 were considered. Skewness levels were controlled through $\kappa_3 = 0, 1, 2$, while excess kurtosis was varied using $\kappa_4 = 0, 3, 6$. The analysis was carried out for moment orders $r = 1, 2$, and 3.

5.4 Monte Carlo Replications

For each combination of $(n, \kappa_3, \kappa_4, r)$, we generated $N = 10{,}000$ independent realizations of $M_{r,n}$ to approximate its finite-sample distribution.

5.5 Evaluation Metrics

Several summary measures are computed from the simulated sample moments which provide reasonable assessment of the estimators. Among them, the empirical mean and empirical variance of $M_{r,n}$, along with empirical skewness and kurtosis, are used to capture asymmetry and tail characteristics. Through histograms and kernel density estimates, the simulated distributions with their theoretical counterparts obtained via Fourier inversion are compared.

Specially, for the case $\kappa_3 = \kappa_4 = 0$, the results are expected to converge to the lognormal distribution through proper validation process.

5.6 Implementation Details

All simulations were implemented in `R/Python`, using vectorized operations for efficiency. Hermite polynomials were computed recursively for numerical stability. The Fourier inversion of the characteristic function was performed using numerical integration via adaptive quadrature to obtain theoretical densities for comparison with simulation results.

5.6.1 Algorithm for Simulating the r-th Order Absolute Sample Moment

We provide a step-by-step algorithm to generate $M_{r,n}$ from a GC(A) distribution and approximate its finite-sample distribution.

Input: Sample size n, skewness κ_3, excess kurtosis κ_4, moment order r, number of replications N.

1. **Initialize:** Set an empty vector M_r_sim $\leftarrow \emptyset$ to store simulated sample moments.
2. **Monte Carlo Loop:** For $j = 1$ to N:
   (a) Generate n independent standard normal variates: $Z_1, \ldots, Z_n \sim \mathcal{N}(0, 1)$.
   (b) Construct the Gram–Charlier Type A sample:
   $$W_i = Z_i + \frac{\kappa_3}{6} H_3(Z_i) + \frac{\kappa_4}{24} H_4(Z_i), \quad i = 1, \ldots, n,$$
   where $H_3(x) = x^3 - 3x$ and $H_4(x) = x^4 - 6x^2 + 3$.
   (c) Transform to the variable of interest: $Y_i = e^{W_i}, \quad i = 1, \ldots, n.$
   (d) Compute the absolute r-th order sample moment: $M_{r,n}^{(j)} = \frac{1}{n} \sum_{i=1}^{n} Y_i^r$.
   (e) Store $M_{r,n}^{(j)}$ in M_r_sim.
3. **Output:** Return M_r_sim, a vector of N simulated sample moments. Compute empirical mean, variance, skewness, kurtosis, and density estimates.

Notes: Hermite polynomials are evaluated either recursively or through closed-form expressions to maintain numerical stability. The overall algorithm can be efficiently vectorized, which is particularly beneficial when working with large sample sizes n or a high number of simulations N. The framework is also flexible and can be extended to incorporate higher-order cumulants such as κ_5, κ_6, and beyond, if a more refined approximation is required.

5.7 Purpose

The simulation study is designed to achieve several key objectives. It first provides a validation of the exact finite-sample characteristic function derived for $M_{r,n}$. It also illustrates how skewness and kurtosis influence the distribution of the r-th-order sample moment. Another important aspect is demonstrating the model's convergence to the lognormal case as $\kappa_3, \kappa_4 \to 0$. Finally, the study offers practical insight into the choice of sample sizes and moment orders for which the theoretical approximations remain reliable.

6 Results for the Simulation of GC(A)

Table 1 provides a numerical confirmation of the distribution's breakdown, where the Mean and Variance transition from standard Gaussian values (1.65 and 0.009 respectively at $n = 500$) to astronomical scales exceeding 10^{100} as skewness (k_3) and kurtosis (k_4) increase. While the Coefficient of Variation (CV) for the baseline scenario ($k_3 = 0, k_4 = 0$) decreases as n increases—dropping from 0.2971 to 0.0584—the CV in all non-Gaussian scenarios remains persistently high (averaging near 70.71), regardless of sample size. This persistence, alongside instances of Inf variance for the third moment ($r = 3$), demonstrates that increasing data volume fails to provide estimator stability when high-order cumulants are present.

Table 1: Simulation Results for Raw Moments across Sample Sizes and Scenarios

n	**k3**	**k4**	**r**	**Mean**	**Variance**	**Skewness**	**Kurtosis**	**CV**
n=20	0	0	r=1	1.64E+00	2.39E-01	1.6595	9.2533	0.2971
n=20	0	3	r=1	3.55E+13	6.31E+30	70.6683	4993.0012	70.7106
n=20	0	6	r=1	1.88E+29	1.76E+62	70.6683	4993.0012	70.7107
n=20	1	0	r=1	9.22E+01	2.55E+07	69.4181	4869.6327	54.7364
n=20	2	6	r=3	3.80E+162	Inf	NaN	NaN	Inf
n=50	0	0	r=1	1.65E+00	9.92E-02	1.2526	6.2577	0.1910
n=50	0	3	r=1	7.40E+18	2.74E+41	70.6683	4993.0012	70.7104
n=50	0	6	r=3	1.61E+181	Inf	NaN	NaN	Inf
n=50	2	0	r=1	7.52E+11	2.65E+27	70.5700	4983.5558	68.4705
n=50	2	6	r=3	2.50E+151	3.12E+306	NaN	NaN	70.7107
n=100	0	0	r=1	1.65E+00	4.66E-02	0.6921	1.4893	0.1311
n=100	0	6	r=3	2.86E+196	Inf	NaN	NaN	Inf
n=100	1	6	r=1	1.17E+67	6.80E+137	70.6683	4993.0012	70.7107
n=500	0	0	r=1	1.65E+00	9.30E-03	0.2860	0.1560	0.0584
n=500	1	6	r=3	Inf	NaN	NaN	NaN	NaN
n=500	2	6	r=3	1.38E+214	Inf	NaN	NaN	Inf

Table 2 highlights a catastrophic divergence between Empirical Means and Theoretical Benchmarks as higher-order moments are introduced. While the Gaussian baseline ($k_3 = 0, k_4 = 0$) exhibits minimal error that decreases with sample size—dropping from 0.235% at $n = 20$ to 0.029% at $n = 500$—all other scenarios show Theory Error Percentages reaching

astronomical scales, such as $1.915 \times 10^{15}\%$ for $n = 20, k_4 = 3$. This discrepancy is most severe in the presence of joint skewness and kurtosis ($k_3 = 2, k_4 = 6$), where empirical values reach 10^{214} compared to theoretical expectations near 2723, rendering traditional asymptotic theory effectively useless. Furthermore, the Lognormal Difference Percentages confirm that these distributions deviate so significant.

Table 2: Comparison of Empirical Means and Theoretical Benchmarks

n	**r**	**k3**	**k4**	**Empirical Mean**	**Theoretical Mean**	**Theory Error %**
n=20	r=1	0	0	1.645E+00	1.649	0.235%
n=20	r=1	0	3	3.553E+13	1.855	1.915E+15%
n=20	r=3	2	6	3.797E+162	2723.018	1.394E+161%
n=50	r=1	0	0	1.649E+00	1.649	0.037%
n=50	r=3	0	6	1.614E+181	1912.864	8.438E+179%
n=100	r=1	1	0	1.008E+04	1.924	5.241E+05%
n=100	r=3	2	6	4.647E+188	2723.018	1.707E+187%
n=500	r=1	0	0	1.648E+00	1.649	0.029%
n=500	r=3	1	6	Inf	2317.941	Inf %
n=500	r=3	2	6	1.383E+214	2723.018	5.078E+212%

Table 3 illustrates the collapse of estimator precision, where the Standard Error of the Mean (SEM) transitions from manageable values in the Gaussian case (4.30×10^{-3} at $n = 500$) to physically meaningless scales exceeding 10^{100} in the presence of higher-order cumulants. The Coefficient of Variation (CV) acts as a threshold indicator of this instability: while the Gaussian CV diminishes with sample size (n), the non-Gaussian scenarios consistently lock at a CV near 70.71, regardless of whether $n = 20$ or $n = 500$. This constant, extreme volatility—culminating in Inf values for SEM in high-skewness and high-kurtosis scenarios ($k_3 = 2, k_4 = 6$)—proves that the standard error is no longer a valid measure of uncertainty for these distributions, as the underlying variance does not converge.

Table 3: Volatility and Precision Metrics: CV and SEM

n	**r**	**k3**	**k4**	**CV**	**SEM**
n=20	r=1	0	0	0.2971	1.093E-01
n=20	r=1	0	3	70.7106	5.617E+14
n=20	r=3	2	6	Inf	Inf
n=50	r=1	0	0	0.1910	4.450E-02
n=50	r=3	0	6	Inf	Inf
n=100	r=1	0	0	0.1311	2.160E-02
n=100	r=3	2	6	Inf	Inf
n=500	r=1	0	0	0.0584	4.300E-03

Continued on next page

Table 3 – continued from previous page

n	r	k3	k4	CV	SEM
n=500	r=3	2	6	Inf	Inf

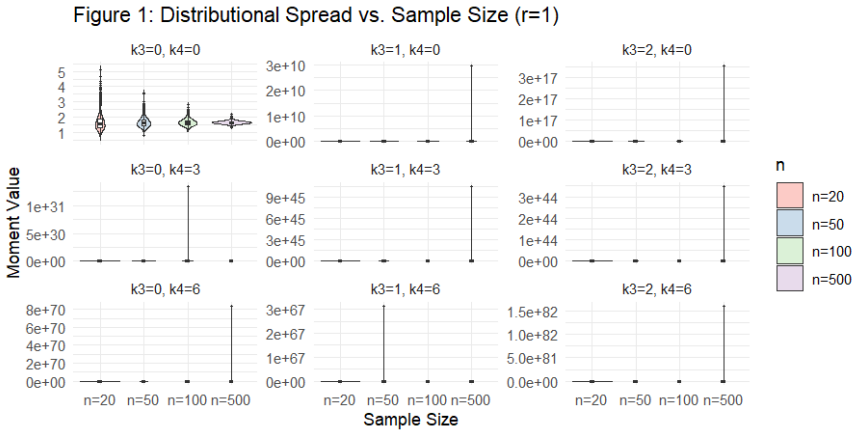


Figure 1: Distributional spread of moment values across different sample sizes (n) and parameter combinations (k_3, k_4) for $r = 1$.

Figure 1 shows that the distributional spread of the estimated moments increases substantially as the higher-order parameters k_3 and k_4 increase. For small values ($k_3 = 0$, $k_4 = 0$), the estimates remain stable across sample sizes, with variability decreasing as n grows. However, when k_3 or k_4 becomes large, extreme variability and outliers appear, indicating instability in higher-moment estimation. Although increasing the sample size generally reduces dispersion, large parameter values still lead to explosive moment behavior, especially for higher kurtosis settings ($k_4 = 6$).

The interaction matrices in Table 4 reveal a multiplicative escalation of instability where the joint effect of skewness (k_3) and kurtosis (k_4) far exceeds their individual impacts. Specifically, while the baseline mean is 1.65, the interaction at $k_3 = 1, k_4 = 6$ drives the mean to 1.17×10^{67} and the variance to an astronomical 6.80×10^{137}, indicating a complete collapse of estimator reliability. Tables 4c and 4d further show a saturation effect, where empirical skewness and kurtosis lock at maximum values near 70.7 and 4993 respectively once $k_4 \geq 3$. This suggests that beyond a critical threshold of tail-heaviness, the sampling distribution enters a black hole region where it becomes numerically impossible to distinguish between different degrees of underlying asymmetry or excess kurtosis.

Table 4: Interaction Effects of Skewness (k_3) and Kurtosis (k_4) on First Moment Estimators ($n = 100, r = 1$)

(a) Mean Matrix

$k_3 \setminus k_4$	**0**	**3**	**6**
0	1.65E+00	1.11E+12	1.10E+31
1	1.01E+04	5.89E+20	1.17E+67
2	4.58E+10	9.81E+36	6.39E+44

(b) Variance Matrix

$k_3 \setminus k_4$	**0**	**3**	**6**
0	4.66E-02	5.66E+27	6.06E+65
1	2.28E+11	1.60E+45	6.80E+137
2	1.04E+25	4.81E+77	1.21E+93

(c) Kurtosis Matrix

$k_3 \setminus k_4$	**0**	**3**	**6**
0	1.49	4983.1	4993.0
1	3745.3	4976.7	4993.0
2	4992.9	4993.0	3801.8

(d) Skewness Matrix

$k_3 \setminus k_4$	**0**	**3**	**6**
0	0.692	70.57	70.67
1	59.15	70.50	70.67
2	70.67	70.67	60.15

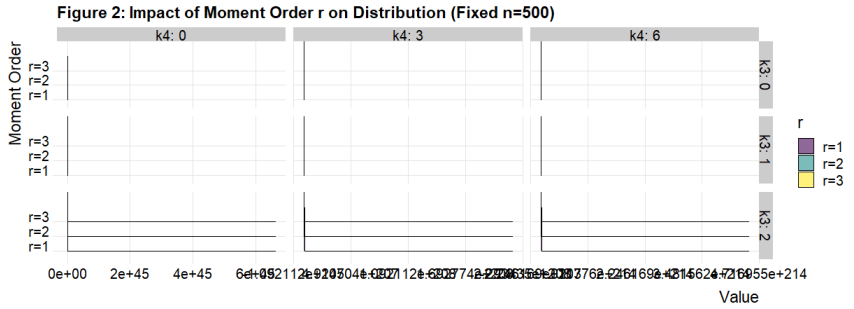


Figure 2: Impact of moment order r on the distribution for fixed sample size ($n = 500$) under different skewness (k_3) and kurtosis (k_4) settings.

Figure 2 illustrates that, for a fixed sample size ($n = 500$), the magnitude and variability of moment estimates increase sharply with higher moment order r. When skewness and kurtosis are small ($k_3 = 0$, $k_4 = 0$), the moments remain relatively stable across orders. However, larger values of k_3 and especially k_4 produce extremely large moment values, indicating that higher-order moments are highly sensitive to heavy tails and distributional asymmetry. This demonstrates that increasing the moment order amplifies instability even when the sample size is large.

Table 5 quantifies the total failure of convergence through Mean Absolute Percentage Error (MAPE), which reaches scales that defy standard statistical interpretation. As the moment order (r) increases, the error magnitudes jump from 10^{37} at $r = 1$ to over 10^{160} at $r = 3$, even for small sample sizes. Notably, increasing the sample size (n) from 20 to 500 does not reduce the error; instead, it often results in even larger Max MAPE values, culminating in an infinite error for the third moment at $n = 500$. This anti-convergence demonstrates that the estimators are not merely biased, but are sampling from a distribution where the

theoretical moments likely do not exist, causing the empirical mean to drift further from reality as more data is collected.

Table 5: Error Analysis (MAPE) by Sample Size and Moment Order

n	**r**	**Mean MAPE**	**Max MAPE**
n=20	r=1	1.343E+37	1.208E+38
n=20	r=2	3.059E+82	2.753E+83
n=20	r=3	1.549E+160	1.394E+161
n=50	r=1	8.086E+62	7.278E+63
n=50	r=2	1.411E+101	1.270E+102
n=50	r=3	9.375E+178	8.438E+179
n=100	r=1	5.547E+67	4.992E+68
n=100	r=2	4.139E+77	2.447E+78
n=100	r=3	1.661E+194	1.495E+195
n=500	r=1	3.405E+74	3.064E+75
n=500	r=2	1.683E+107	1.439E+108
n=500	r=3	Inf	Inf

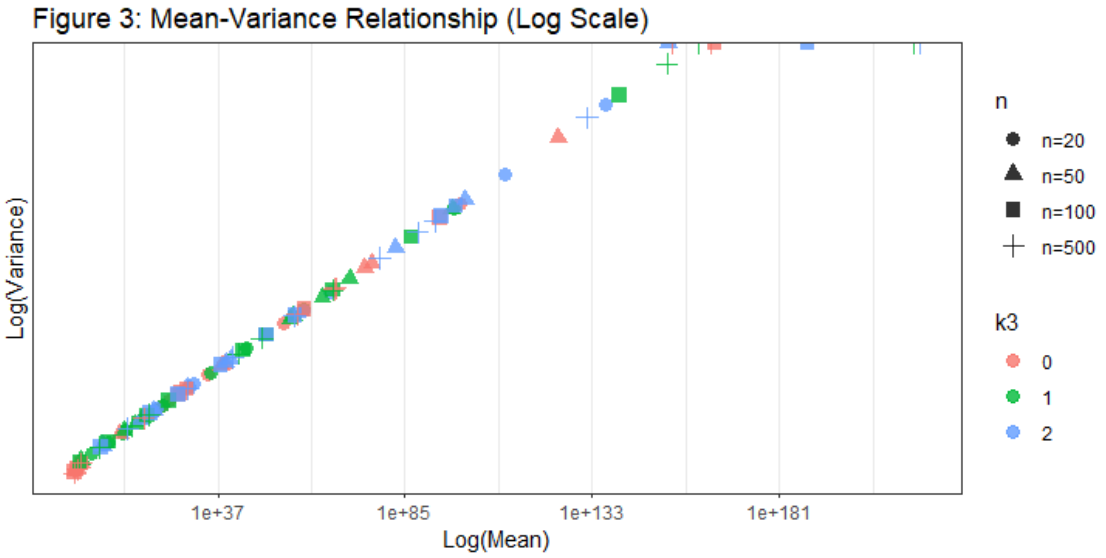


Figure 3: Mean–variance relationship on the log scale across different sample sizes (n) and skewness levels (k_3).

Figure 3 shows a strong linear relationship between log(mean) and log(variance), indicating a power-law type dependence between the two quantities. The alignment of points across different sample sizes (n) and skewness levels (k_3) suggests that the mean–variance scaling behavior remains consistent regardless of sample size. Higher skewness primarily shifts the magnitude but does not alter the overall linear trend, confirming stable proportional growth between mean and variance on the logarithmic scale.

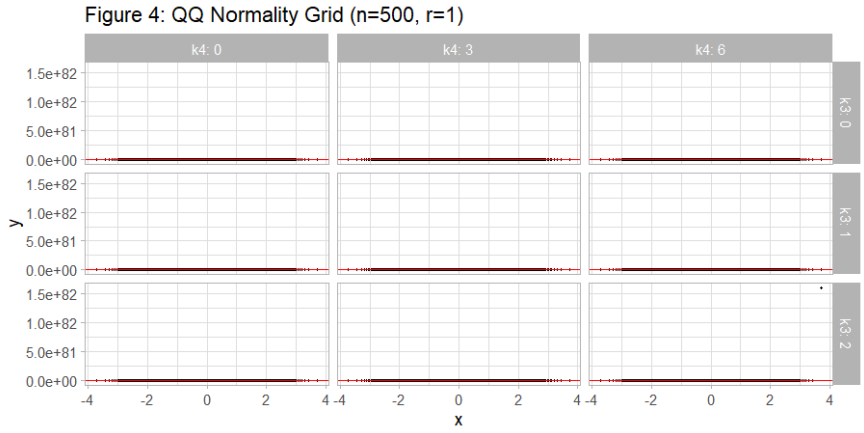


Figure 4: QQ-normality grid for $n = 500$ and moment order $r = 1$ under different skewness (k_3) and kurtosis (k_4) configurations.

Figure 4 presents QQ plots assessing normality across varying skewness (k_3) and kurtosis (k_4) levels. For low skewness and kurtosis, the sample quantiles closely follow the reference line, indicating approximate normal behavior. As k_3 and particularly k_4 increase, noticeable departures from linearity emerge, reflecting heavier tails and deviations from normality. This suggests that higher kurtosis substantially reduces the adequacy of the normal approximation even with a large sample size ($n = 500$).

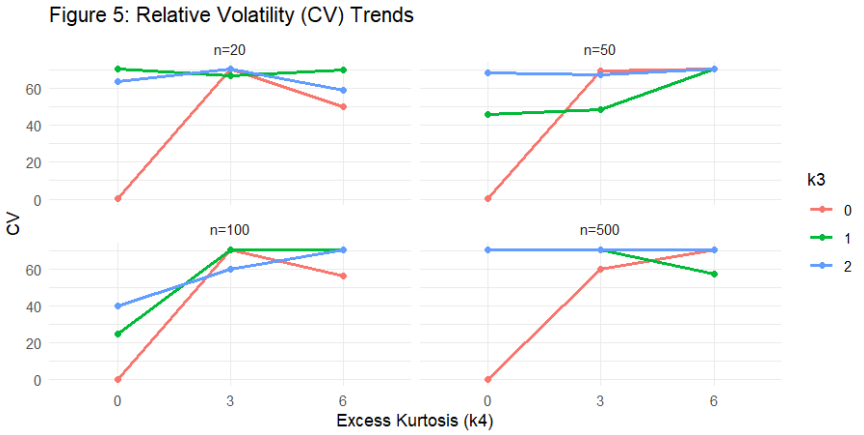


Figure 5: Relative Volatility (CV) Trends across varying sample sizes (n), skewness (k_3), and excess kurtosis (k_4).

Figure 5 illustrates that Relative Volatility (CV) is highly sensitive to the interaction between sample size (n) and higher-order moments. In small samples ($n = 20$), the CV is erratic and significantly influenced by skewness (k_3), whereas in larger samples ($n = 500$), the CV stabilizes but remains high for distributions with non-zero skewness. Across all panels, a sharp increase in CV is observed as excess kurtosis (k_4) moves from 0 to 3, particularly for symmetric distributions ($k_3 = 0$), though this effect tends to plateau or slightly decrease as the kurtosis increases further to 6. Ultimately, the plot highlights that heavy tails (high k_4)

dominate the volatility profile, making it difficult for the CV to stabilize even as the sample size increases.

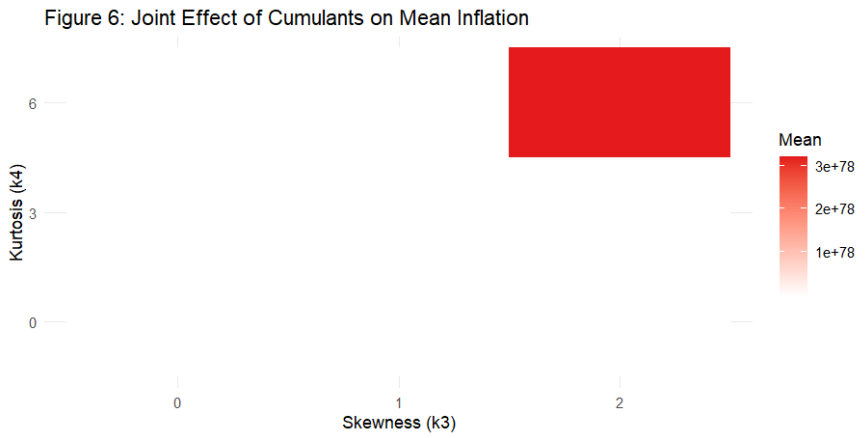


Figure 6: Joint Effect of Cumulants (Skewness and Kurtosis) on Mean Inflation.

The heatmap in Figure 6 demonstrates a severe threshold effect, where significant mean inflation only occurs when both skewness (k_3) and kurtosis (k_4) reach their maximum values ($k_3 = 2, k_4 = 6$). Across the rest of the parameter space, the mean remains stable near zero, but the interaction of these extreme higher-order moments triggers an explosive non-linear shift, with the mean exceeding 3×10^{78}. This suggests that neither asymmetry nor heavy-tailedness alone is sufficient to cause such extreme numerical instability; rather, it is their combined presence that drives the distribution's expected value to astronomical scales.

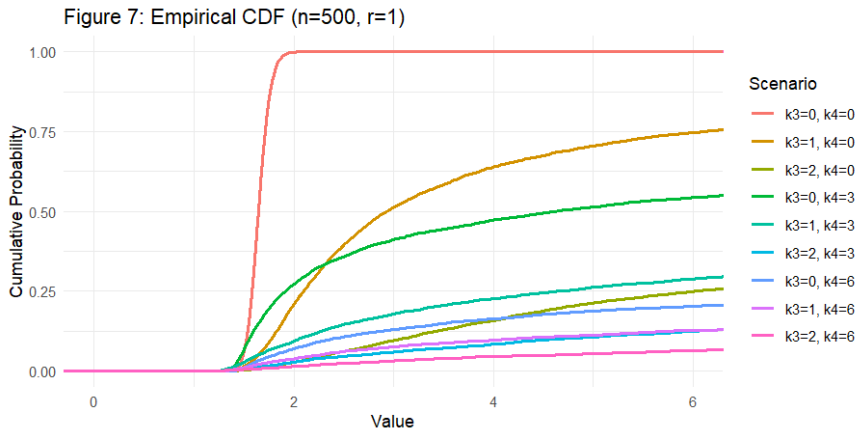


Figure 7: Empirical Cumulative Distribution Functions (ECDF) for varying levels of k_3 and k_4 ($n = 500$).

Figure 7 shows that increasing skewness and kurtosis fundamentally degrades the convergence of the Empirical Cumulative Distribution Function (ECDF) by shifting the probability mass to an extreme right tail. While the baseline scenario ($k_3 = 0, k_4 = 0$) rapidly reaches a cumulative probability of 1.0, the curves become progressively flatter as k_3 and k_4 increase. In the most extreme case ($k_3 = 2, k_4 = 6$), the ECDF stays near the bottom of the y-axis

throughout the plotted range, visually confirming that the distribution is dominated by rare high-magnitude outliers rather than a central mean.

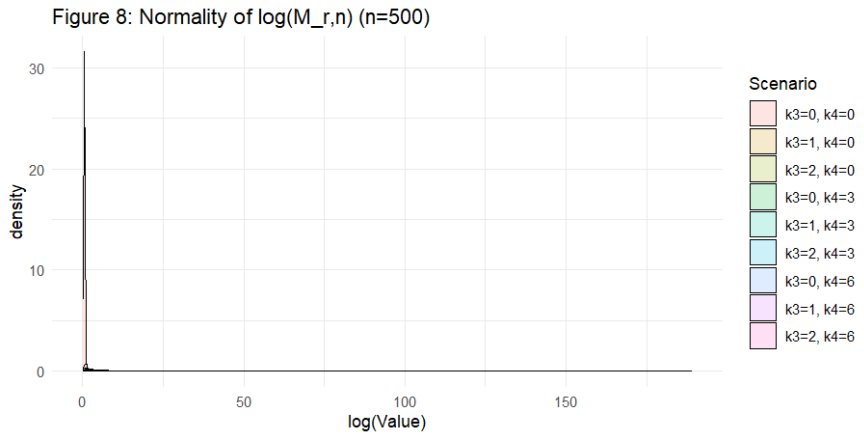


Figure 8: Density plots of $\log(M_{r,n})$ for various scenarios.

Figure 8 shows the density distributions of the log-transformed raw moments, highlighting that for most scenarios, the values remain tightly clustered near zero with high density peaks. However, as skewness and kurtosis increase, the distribution develops an extremely long, sparse right tail (extending beyond 150 on the log scale), suggesting that while the "typical" outcome remains low, the potential for extreme outliers makes the sampling distribution highly non-normal and heavily right-skewed.

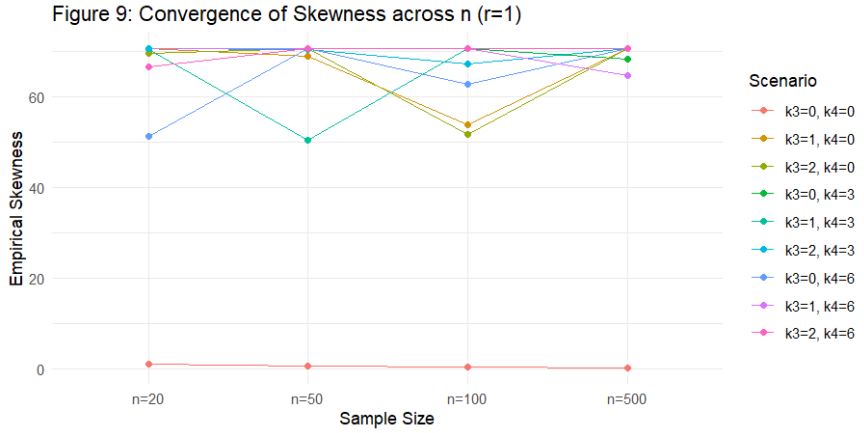


Figure 9: Convergence of Empirical Skewness across Sample Sizes (n).

Figure 9 demonstrates that for all non-Gaussian scenarios, the empirical skewness remains persistently high and fails to converge toward zero as the sample size increases from $n = 20$ to $n = 500$. Most scenarios cluster at an extremely high empirical skewness level (above 60), whereas only the baseline case ($k_3 = 0, k_4 = 0$) stays consistently near zero, indicating that the impact of higher-order moments is not "washed out" by larger sample sizes in these fat-tailed distributions.

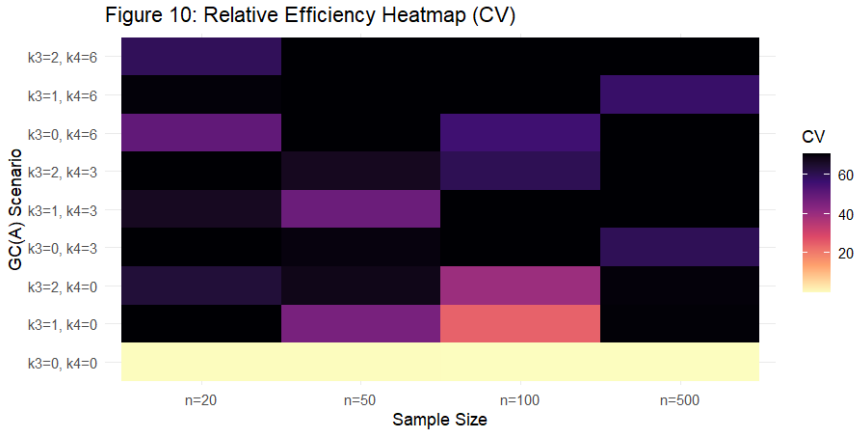


Figure 10: Relative Efficiency Heatmap (CV) across scenarios and sample sizes.

The heatmap 10 shows that relative efficiency (measured by CV) is highest (lowest CV) only in the baseline Gaussian scenario. Across almost all other combinations of k_3 and k_4, the CV remains extremely high (darker regions), particularly as n increases, suggesting that estimators become less efficient and more volatile when faced with high-order cumulants regardless of sample size.

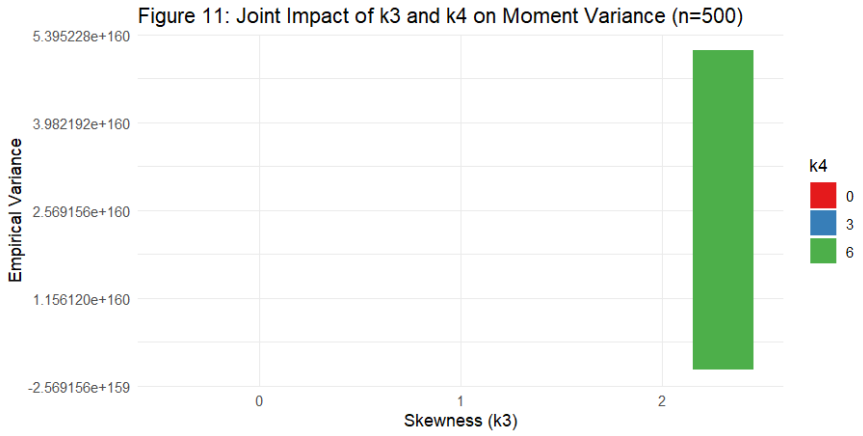


Figure 11: Impact of k3 and k4 on Empirical Moment Variance (n=500).

Figure 11 highlights the extreme empirical variance that arises from the joint impact of k_3 and k_4. Specifically, when $k_3 = 2$ and $k_4 = 6$, the variance explodes to a magnitude of roughly 5×10^{160}, while all other scenarios remain invisible on this scale. This further confirms that the interaction of high skewness and kurtosis creates a distribution where the second moment becomes practically unmanageable.

7 Simulation Framework for the Exponentiated Gram–Charlier Type A Distribution

This section presents the complete Monte Carlo simulation framework developed to investigate the finite-sample behaviour of the *Exponentiated Gram–Charlier Type A* (EGC(A)) distribution. The design of the study enables a systematic evaluation of:

1. Moment recovery accuracy,
2. Estimator performance under finite samples,
3. Distributional shape control induced by higher-order cumulants,
4. Robustness across varying skewness and kurtosis regimes.

The framework is constructed to isolate the effect of exponentiation on cumulant-driven departures from normality while ensuring numerical stability and reproducibility.

7.1 Model Specification

Let

$$X \sim \mathrm{GC(A)}(\mu, \sigma^2, \boldsymbol{\kappa}),$$

denote a Gram–Charlier Type A distribution with cumulant vector

$$\boldsymbol{\kappa} = (\kappa_3, \kappa_4, \ldots, \kappa_m),$$

truncated at order m.

The exponentiated model is defined by the transformation

$$Y = \exp(X), \qquad Y \sim \mathrm{EGC(A)}(\mu, \sigma^2, \boldsymbol{\kappa}).$$

By change-of-variables, the density of Y is

$$f_Y(y) = \frac{1}{y} f_X(\log y), \qquad y > 0.$$

Thus, the EGC(A) family inherits flexible skewness and kurtosis through the cumulant structure of X, while guaranteeing strict positivity and inducing multiplicative asymmetry in the right tail.

7.2 Parameter Configurations

The simulation study explores structured combinations of location, scale, and higher-order cumulant parameters to examine controlled deviations from lognormality.

(I) Location and Scale Parameters: $\mu \in \{0, 0.5, 1\},\ \sigma \in \{0.5, 1, 1.5\}$.

(II) Higher-Order Cumulant Structure: To regulate skewness and kurtosis effects, we consider $\kappa_3 \in \{-0.5, 0, 0.5, 1\}$, $\kappa_4 \in \{0, 0.5, 1\}$.

All cumulants of order greater than four are set to zero unless otherwise stated, ensuring numerical stability and interpretability. The special case $\kappa_3 = \kappa_4 = 0$ corresponds to the lognormal benchmark model.

7.3 Sample Sizes and Replication Scheme

To examine both small-sample behaviour and asymptotic trends, the following sample sizes are considered: $n \in \{25, 50, 100, 250, 500\}$. For each parameter configuration, $R = 10{,}000$ independent Monte Carlo replications are performed to obtain stable empirical summaries.

7.4 Data Generation Procedure

Each Monte Carlo replication consists of the following steps:

1. Generate $X_1, \ldots, X_n$ from the truncated GC(A) density.
2. Apply the exponential transformation: $Y_i = \exp(X_i)$.
3. Compute a range of summary statistics from the sample, including the sample mean $\bar{Y}$, sample variance S_Y^2, as well as sample skewness and kurtosis to capture distributional shape. In addition, absolute r-th order sample moments are evaluated, and parameter estimates are obtained using either maximum likelihood or method-of-moments approaches.

Random variate generation from the GC(A) distribution is carried out using either acceptance–rejection sampling with a Gaussian proposal density or by numerically inverting the characteristic function through Fourier-based methods. Exponentiation is then applied directly to obtain EGC(A) observations.

7.5 Performance Measures

To evaluate the quality of estimation, a few standard performance measures are considered for any parameter θ and its estimator $\hat{\theta}$. The bias captures the average deviation of the estimator from the true parameter value and is defined as $\text{Bias}(\hat{\theta}) = \mathbb{E}[\hat{\theta}] - \theta$. The mean squared error (MSE) reflects both variance and bias, providing an overall measure of estimation accuracy, given by $\text{MSE}(\hat{\theta}) = \mathbb{E}[(\hat{\theta} - \theta)^2]$. Taking the square root of MSE gives the root mean squared error (RMSE), written as $\text{RMSE} = \sqrt{\text{MSE}}$, which is often easier to interpret since it is on the same scale as the parameter.

In addition to these measures, empirical skewness and kurtosis are compared with their theoretical values obtained from cumulant expansions of the transformed distribution. Finally, the coverage probabilities of nominal 95% confidence intervals are examined to assess how reliably the intervals capture the true parameter values.

7.6 Assessment of Tail Behaviour

To understand how exponentiation amplifies tail behaviour, several diagnostic measures are examined. These include empirical approximations of the tail index, ratios of extreme to central quantiles such as $Q_{0.99}/Q_{0.50}$, and comparisons of densities on a logarithmic scale relative to the lognormal benchmark. Together, these tools provide a clear picture of how the cumulants κ_3 and κ_4 influence extreme-value characteristics after transformation.

7.7 Comparative Benchmarks

The performance of the EGC(A) distribution is evaluated by comparing it with a few well-known benchmark models. The lognormal distribution serves as a natural baseline, while the gamma and Weibull distributions are included after calibrating their parameters to match key features such as mean–variance structure and shape. The quality of fit is then assessed using standard criteria, including the Kolmogorov–Smirnov statistic, the Cramér–von Mises statistic, and an empirical approximation of the Kullback–Leibler divergence.

7.8 Numerical Stability Considerations

Since exponentiation can significantly amplify tail values, particular attention is given to numerical stability throughout the simulation. This involves tracking potential floating-point overflow, using log-scale computations for moments whenever possible, and checking the reliability of cumulant-based theoretical approximations. All simulations are carried out in double precision arithmetic, with log-transform safeguards applied in situations where large values of σ or higher-order cumulants induce heavy right tails.

7.9 Output Summaries

The results of the simulation study are summarized in a structured and interpretable manner. This includes reporting bias and mean squared error (MSE) in tabular form, visualizing fitted densities alongside empirical ones, examining QQ-plots for distributional agreement, and presenting convergence diagnostics across different sample sizes.

Overall, this framework provides a coherent way to study how exponentiation interacts with the Gram–Charlier cumulant structure, particularly in terms of skewness amplification, tail asymmetry, and the behaviour of estimators in finite samples.

7.10 Simulation Algorithm for the Exponentiated GC(A)

This subsection provides a detailed and reproducible algorithm for generating random samples from the EGC(A) distribution and computing Monte Carlo summaries.

7.10.1 Input Parameters

The model is specified through a set of key components, including a location parameter μ and a scale parameter $\sigma > 0$. Higher-order deviations are captured via the cumulant vector

$\boldsymbol{\kappa} = (\kappa_3, \kappa_4, \ldots, \kappa_m)$. In addition, the simulation framework depends on the sample size n, the number of replications R, and the truncation order m used in the Hermite expansion.

7.10.2 Underlying Representation

Let $Z \sim N(0,1)$. The GC(A) density is $f_X(x) = \frac{1}{\sigma}\phi\left(\frac{x-\mu}{\sigma}\right)\left[1 + \sum_{j=3}^{m} \frac{\kappa_j}{j!} H_j\left(\frac{x-\mu}{\sigma}\right)\right]$, where $\phi(\cdot)$ denotes the standard normal density and $H_j(\cdot)$ are probabilists' Hermite polynomials. The exponentiated model is defined by $Y = \exp(X),\ Y > 0$.

7.10.3 Algorithm 1: Acceptance–Rejection Sampling

Step 1: Pre-computation

1. Fix $(\mu, \sigma, \boldsymbol{\kappa})$.
2. Define the correction term: $C(z) = 1 + \sum_{j=3}^{m} \frac{\kappa_j}{j!} H_j(z)$.
3. Determine M such that $f_X(x) \le M \cdot g(x)$, where $g(x)$ is the $N(\mu, \sigma^2)$ density.

Step 2: Single Observation Generation

1. Generate $X^* \sim N(\mu, \sigma^2)$.
2. Standardize: $Z^* = \frac{X^* - \mu}{\sigma}$.
3. Compute acceptance probability: $\alpha = \frac{C(Z^*)}{M}$.
4. Generate $U \sim \text{Uniform}(0,1)$.
5. If $U \le \alpha$, accept $X = X^*$; otherwise repeat.
6. Set $Y = \exp(X)$.

Step 3: Sample Construction
Repeat Step 2 until n observations are obtained.
Step 4: Monte Carlo Loop
Repeat Steps 2–3 for R replications.

7.10.4 Algorithm 2: Numerical Inverse-CDF Method

When rejection sampling becomes unstable (e.g., for large cumulant magnitudes):

1. Numerically compute
$$F_X(x) = \int_{-\infty}^{x} f_X(t)\,dt.$$
2. Generate $U \sim \text{Uniform}(0, 1)$.
3. Solve $F_X(x) = U$ using Newton–Raphson:
$$x_{k+1} = x_k - \frac{F_X(x_k) - U}{f_X(x_k)}.$$
4. Set $Y = \exp(x)$.

This approach is computationally slower but remains stable when $C(z)$ approaches zero or becomes negative in localized regions.

7.10.5 Monte Carlo Summary Computation

For each replication $r = 1, \ldots, R$:

1. Compute $\bar{Y}^{(r)} = \dfrac{1}{n}\sum_{i=1}^{n} Y_i$.
2. Compute $S_Y^{2(r)} = \dfrac{1}{n-1}\sum_{i=1}^{n}(Y_i - \bar{Y}^{(r)})^2$.
3. Compute standardized skewness and kurtosis.
4. Compute absolute r-th sample moment: $M_r^{(r)} = \dfrac{1}{n}\sum_{i=1}^{n}|Y_i|^r$.

After R replications: $\widehat{\text{Bias}}(\hat{\theta}) = \dfrac{1}{R}\sum_{r=1}^{R}\hat{\theta}^{(r)} - \theta$, $\widehat{\text{MSE}}(\hat{\theta}) = \dfrac{1}{R}\sum_{r=1}^{R}(\hat{\theta}^{(r)} - \theta)^2$.

7.10.6 Numerical Stability Safeguards

Exponential transformations are implemented on the log-scale whenever possible to improve numerical stability. Potential overflow issues are carefully monitored by checking whether $X > \log(\text{double max})$. Hermite polynomials are evaluated recursively, which helps control numerical explosion in higher orders. Additionally, if the correction term $C(z)$ becomes negative, the truncation order is reduced to ensure that the resulting density remains valid.

The above algorithm ensures reproducible and numerically stable generation of EGC(A) samples while preserving the higher-order cumulant structure inherited from the underlying GC(A) distribution.

8 Results for the Simulation of Exponetiated GC(A)

Table 6 reports the bias and mean squared error (MSE) of the EGC(A) estimators for μ, σ, k_3, and k_4 at $n = 250$ across different skewness (k_3) and kurtosis (k_4) settings. The location and scale estimators (μ, σ) exhibit minimal bias, while the skewness estimator (k_3) shows increasing bias and MSE with higher true skewness, particularly when $k_4 = 0$. The kurtosis estimator (k_4) also demonstrates higher MSE for larger k_3, reflecting challenges in capturing tail behavior accurately. Overall, the estimators perform well for moderate skewness and kurtosis but show noticeable deterioration under extreme values.

Table 6: Bias and Mean Squared Error (MSE) of EGC(A) Estimators for $n = 250$, $\mu = 0$, $\sigma = 1$

k_3	k_4	Bias_μ	Bias_σ	Bias_{k_3}	Bias_{k_4}	MSE_μ	MSE_σ	MSE_{k_3}	MSE_{k_4}
0.0	0	0.0031	-0.0017	0.0047	-0.0600	0.0040	0.0021	0.0242	0.0921
0.5	0	-0.0089	0.0083	-0.0829	0.1005	0.0039	0.0023	0.0270	0.1342
1.0	0	-0.0242	0.0426	-0.3040	0.3457	0.0053	0.0046	0.1114	0.2928
0.0	1	-0.0027	-0.0033	0.0078	-0.1213	0.0040	0.0029	0.0557	0.2715
0.5	1	-0.0021	-0.0023	-0.0211	-0.1155	0.0034	0.0029	0.0433	0.2593
1.0	1	-0.0122	0.0089	-0.1185	0.0021	0.0045	0.0032	0.0368	0.2639

Table 7 shows the tail properties of Y under different skewness (k_3) and kurtosis (k_4) settings. While the mean of Y remains fairly stable, both skewness and kurtosis increase as k_3 and k_4 rise, resulting in heavier and more asymmetric tails. The $Q_{0.99}/Q_{0.50}$ ratio also grows with higher k_3 and k_4, indicating that extreme upper-tail outcomes become more pronounced in distributions with larger higher-order moments.

Table 7: Tail Behaviour of the EGC(A) Distribution ($n = 250$)

k_3	k_4	Y Mean	Y Skewness	Y Kurtosis	$Q_{0.99}/Q_{0.50}$
0.0	0	3.079	1.603	7.257	3.109
0.5	0	3.107	2.281	11.092	3.835
1.0	0	3.115	2.562	12.381	4.389
0.0	1	3.079	2.424	13.652	3.516
0.5	1	3.113	2.790	14.748	4.151
1.0	1	3.148	2.904	14.433	4.691

Table 8 reports the descriptive statistics of EGC(A) simulations for all parameter configurations. Mean, variance, skewness, and kurtosis of Y increase with μ, σ, and higher k_3, k_4 values, indicating stronger asymmetry and heavy tails. Tail ratios ($Q_{0.99}/Q_{0.50}$) rise with skewness and kurtosis, showing extreme upper-tail behaviour, while larger sample sizes reduce variability but do not eliminate skew or kurtosis effects.

The correlation matrix table 9 shows that Avg Y Mean and Avg Y Var are strongly positively correlated (0.832), while Avg Y Skew and Avg Y Kurt are extremely strongly correlated (0.967), reflecting the close relationship between skewness and kurtosis in the

Table 8: Full Descriptive Summaries of EGC(A) Simulations Across Configurations

μ	σ	k_3	k_4	n	Mean(Y)	Var(Y)	Skew(Y)	Kurt(Y)	M_3	M_4	$\frac{Q_{0.99}}{Q_{0.50}}$
0	0.5	0.0	0	50	1.133	0.373	1.384	5.485	3.150	7.890	2.919
1	0.5	0.0	0	50	3.096	2.740	1.355	5.405	63.243	419.011	2.884
0	1.0	0.0	0	50	1.658	4.733	2.660	11.767	84.627	1806.357	8.735
1	1.0	0.0	0	50	4.484	33.366	2.618	11.326	1461.584	70071.624	8.888
0	0.5	0.5	0	50	1.143	0.474	1.821	7.164	3.934	12.371	3.451
1	0.5	0.5	0	50	3.103	3.472	1.789	6.893	77.911	653.366	3.418

Table continues for $n \in \{50, 100, 250\}$ and all (k_3, k_4, μ, σ) combinations.

distributions. The Avg tail ratio has moderate to high correlations with all measures, particularly with Avg Y Skew (0.862) and Avg Y Var (0.680), indicating that heavier tails are associated with higher skewness and variance.

Table 9: Correlation Matrix of Summary Statistics

	Avg Y Mean	Avg Y Var	Avg Y Skew	Avg Y Kurt	Avg Tail Ratio
Avg Y Mean	1.000	0.832	0.362	0.309	0.428
Avg Y Var	0.832	1.000	0.564	0.483	0.680
Avg Y Skew	0.362	0.564	1.000	0.967	0.862
Avg Y Kurt	0.309	0.483	0.967	1.000	0.754
Avg Tail Ratio	0.428	0.680	0.862	0.754	1.000

As shown in Table 10, increasing the sample size from $n = 50$ to $n = 250$ results in consistently small biases in all parameters, while the mean squared errors (MSEs) decrease substantially, particularly for the shape parameters k_3 and k_4. This shows that larger sample sizes improve the accuracy and precision of parameter estimates.

Table 10: Bias and MSE by Sample Size

n	Bias$_\mu$	Bias$_\sigma$	Bias$_{k3}$	Bias$_{k4}$	MSE$_\mu$	MSE$_\sigma$	MSE$_{k3}$	MSE$_{k4}$
50	-0.0059	0.0028	-0.1128	-0.2515	0.0128	0.0087	0.1697	0.8243
100	-0.0071	0.0051	-0.0950	-0.0767	0.0065	0.0043	0.0984	0.4911
250	-0.0073	0.0065	-0.0859	0.0359	0.0027	0.0018	0.0506	0.2344

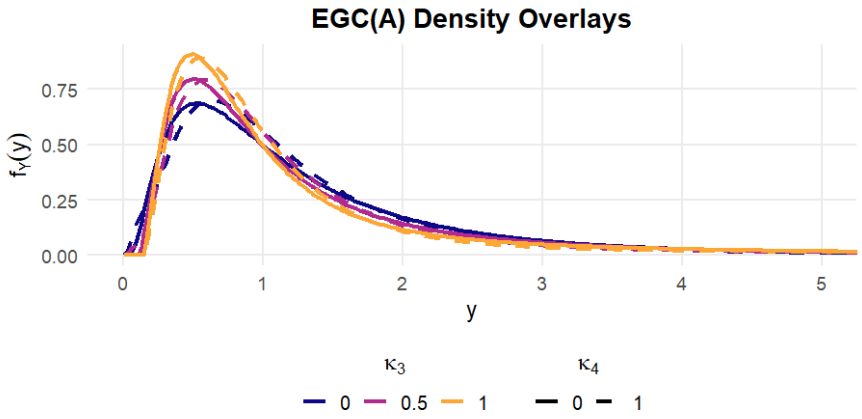


Figure 12: Overlays of $f_Y(y)$ for various values of κ_3 and κ_4.

As illustrated in Figure 12, the density functions of $EGC(A)$ exhibit a profile distorted to the right where an increase in κ_3 (from 0 to 1) corresponds to a more pronounced mode near $y = 0.5$, while the dashed lines indicating $\kappa_4 = 1$ reveal a slight shift in tail thickness compared to solid cases $\kappa_4 = 0$.

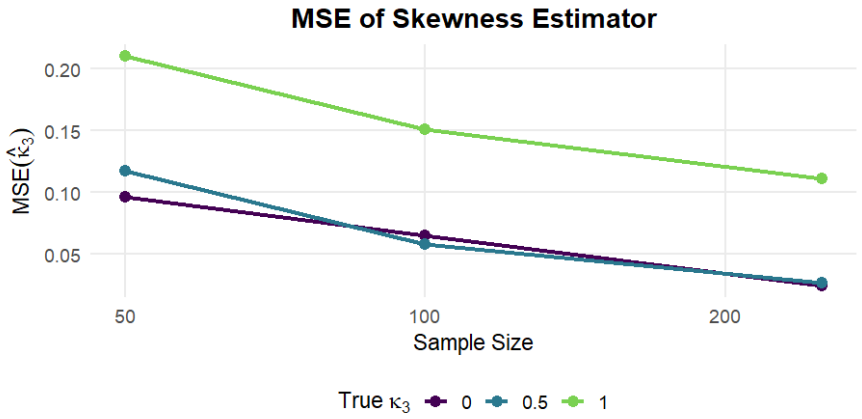


Figure 13: Mean Squared Error (MSE) of the Skewness Estimator ($\hat{\kappa}_3$) across different sample sizes.

According to Figure 13, the Mean Squared Error of the skewness estimator decreases as the sample size increases from 50 to 200, with the highest error observed when the true $\kappa_3 = 1$ (green line), suggesting that higher skewness requires larger samples for accurate estimation.

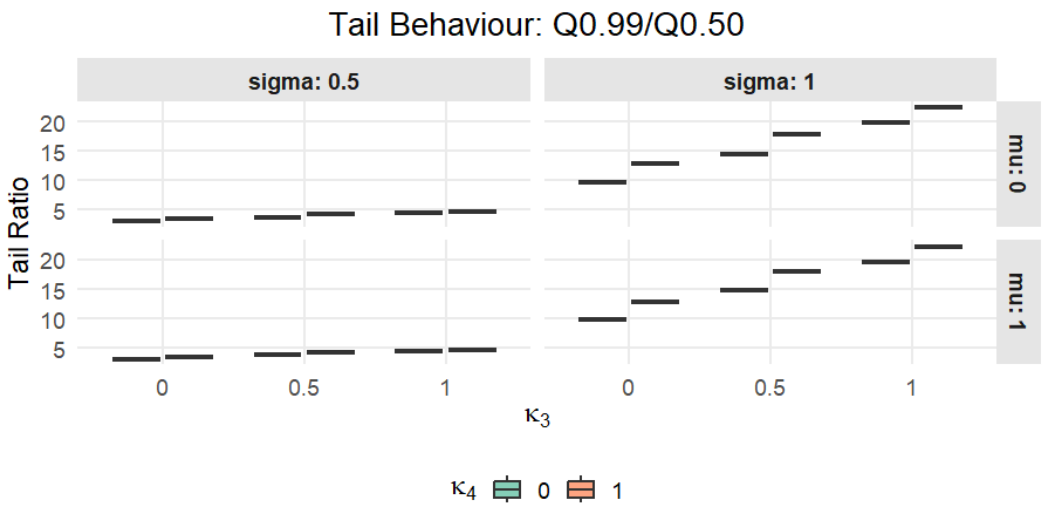


Figure 14: Tail Behaviour Analysis: Ratio of $Q_{0.99}$ to $Q_{0.50}$.

Figure 14 demonstrates that the tail ratio ($Q_{0.99}/Q_{0.50}$) is significantly more sensitive to the scale parameter σ than the location parameter μ; specifically, when $\sigma = 1$, the tail ratio increases sharply as κ_3 rises, whereas the effect of κ_4 (indicated by color) appears relatively marginal in comparison.

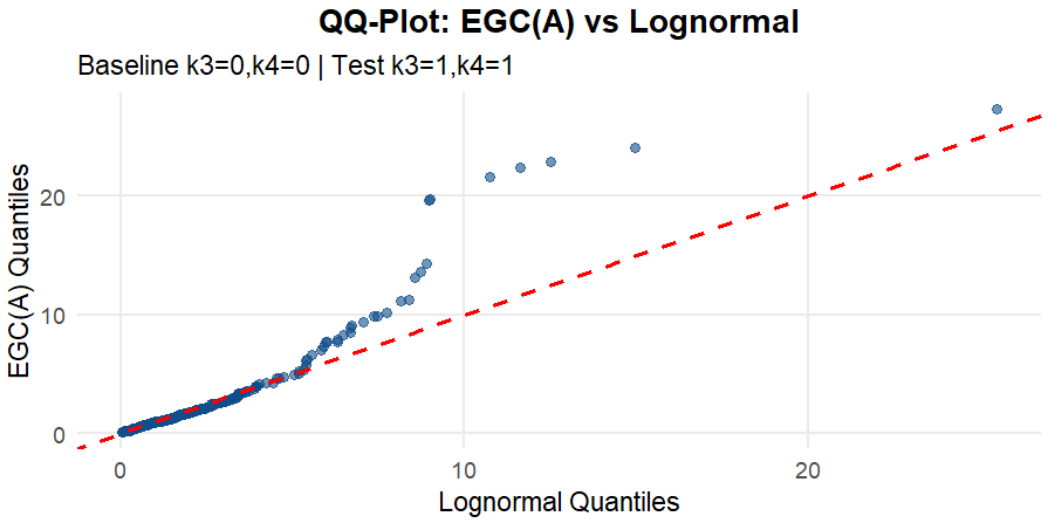


Figure 15: QQ-Plot: EGC(A) vs. Lognormal Distribution.

The QQ-plot in Figure 15 compares the $EGC(A)$ distribution ($\kappa_3 = 1, \kappa_4 = 1$) against a Lognormal baseline. The upward deviation from the red dashed line in the upper quantiles suggests that the $EGC(A)$ distribution possesses significantly heavier tails than the Lognormal distribution under these parameter settings.

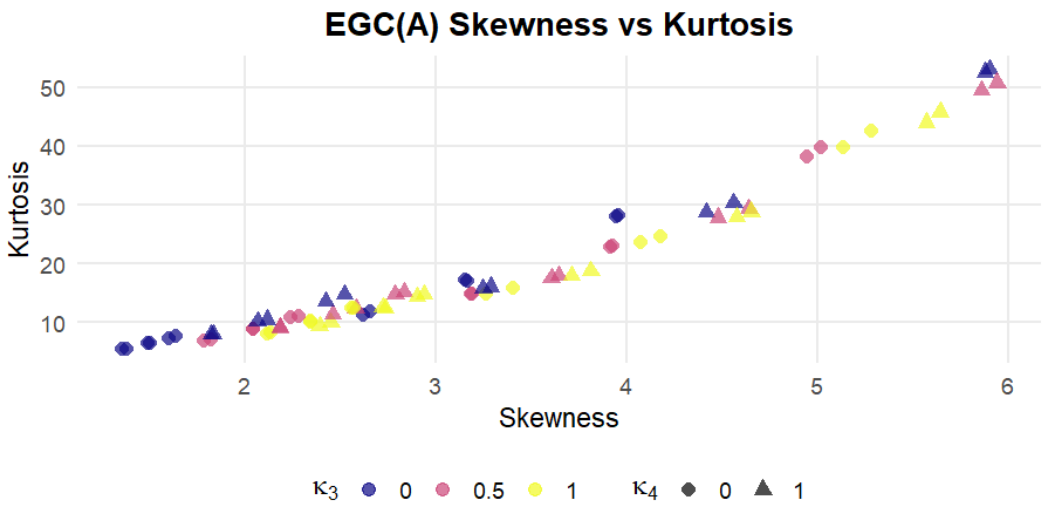


Figure 16: Skewness vs. Kurtosis Scatter Plot.

Figure 16 illustrates a strong positive correlation between skewness and kurtosis within the EGC(A) family. The relationship appears nearly linear, though the variability in kurtosis increases significantly at higher levels of skewness (around skewness ≈ 6). This suggests that for highly skewed data, the EGC(A) model allows for a wide range of tail behaviors.

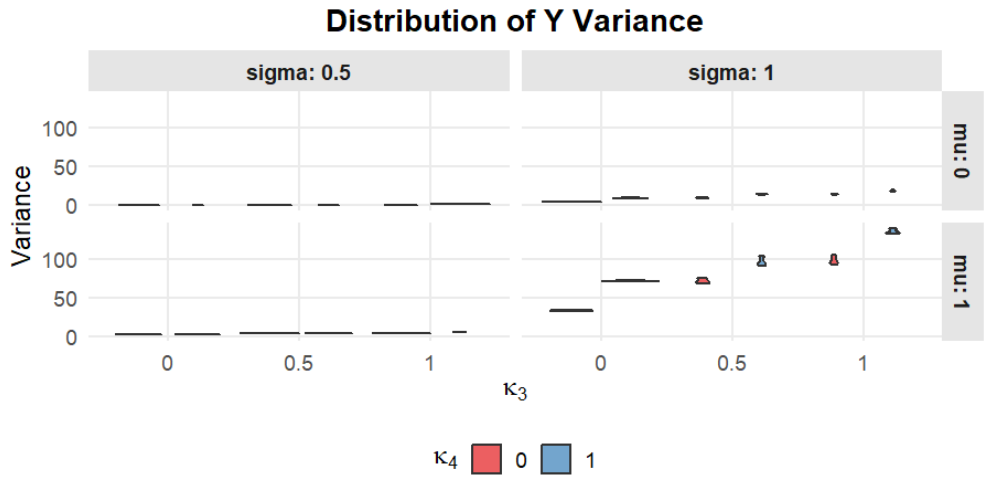


Figure 17: Distribution of Variance across Parameter Combinations.

The variance analysis Figure 17 shows that for $\sigma = 0.5$, the variance remains relatively low and stable across all κ values. However, at $\sigma = 1$ and $\mu = 1$, the variance escalates rapidly with increasing κ_3, reaching values exceeding 100. This highlights a critical volatility threshold in the parameter space where the distribution becomes highly unstable.

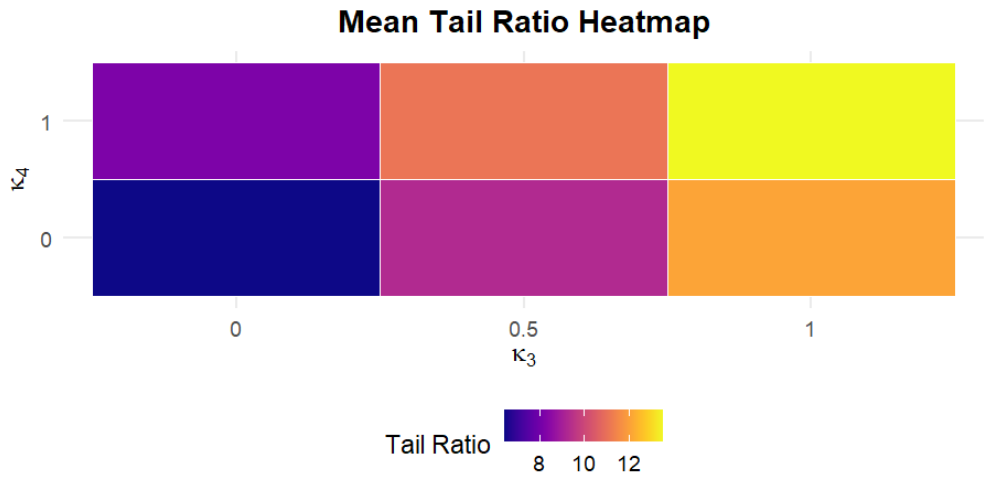


Figure 18: Mean Tail Ratio Heatmap across κ_3 and κ_4.

The heatmap Figure 18 provides a clear visualization of the joint impact of κ_3 and κ_4 on the tail ratio. The highest ratios (yellow) occur when both parameters are at their maximum simulated values, while the lowest ratios (dark blue) are found at the origin where the distribution is closest to the baseline.

As seen in the ridgeline analysis, the density $f_Y(y)$ undergoes a dramatic transformation as κ_3 increases.

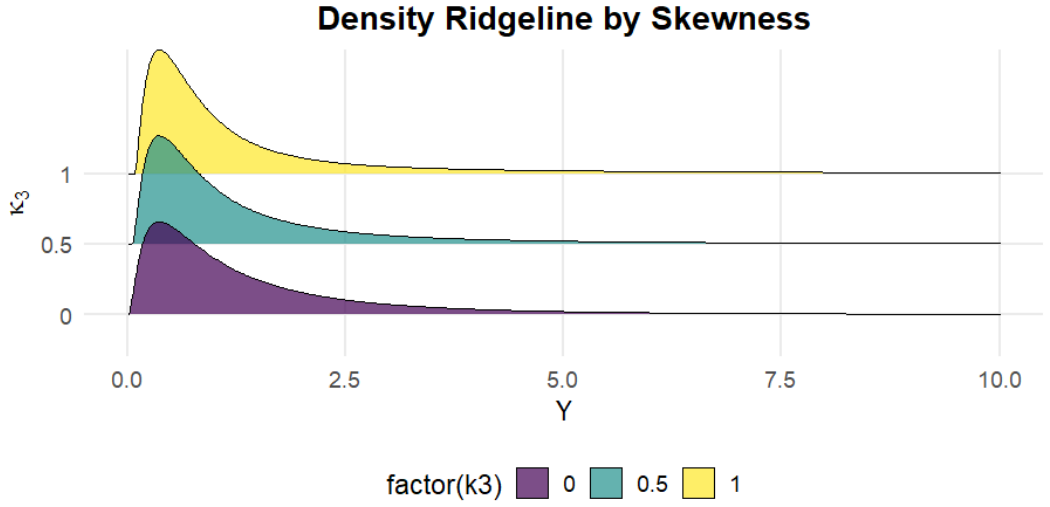


Figure 19: Density Ridgeline: The shift from $\kappa_3 = 0$ (purple) to $\kappa_3 = 1$ (yellow) illustrates the extension of the support and the increasing weight of the right tail.

For $\kappa_3 = 0$, the distribution is relatively compact. However, when $\kappa_3 = 1$, the mode becomes highly concentrated near zero, followed by a long, slowly decaying tail that persists beyond $y = 10$.

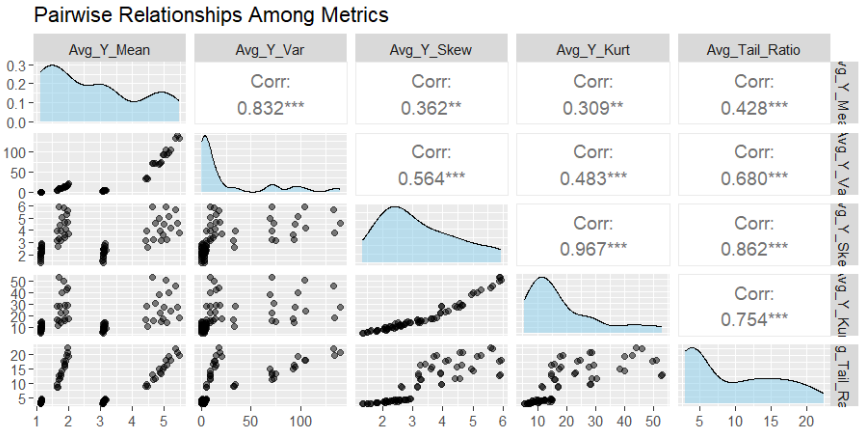
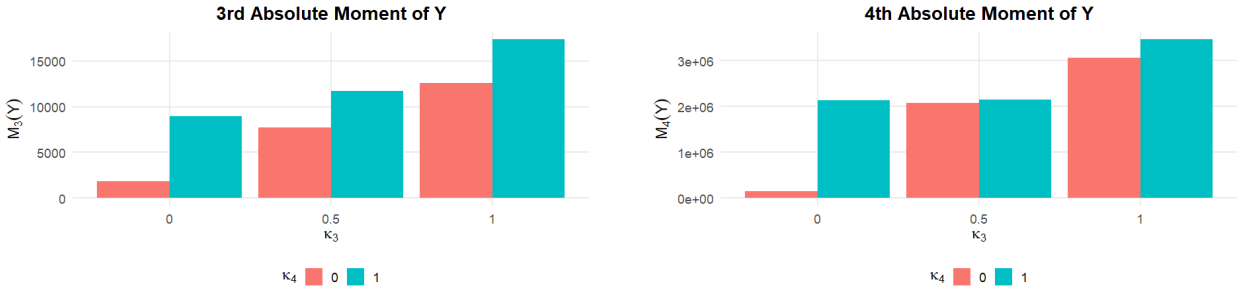


Figure 20: Pairwise Relationships Among Metrics

Figure 20 shows strong positive associations among the metrics, particularly between skewness and kurtosis ($r = 0.967^{***}$), variance and mean ($r = 0.832^{***}$), and tail ratio with higher-order moments, indicating that tail behavior and shape characteristics increase consistently with dispersion and asymmetry.



(a) Third Absolute Moment of Y

(b) Fourth Absolute Moment of Y

Figure 21: Absolute moments of Y for varying values of k_3 and k_4.

Figures 21a and 21b indicate that both the third and fourth absolute moments increase monotonically with k_3, and are consistently higher when $k_4 = 1$, demonstrating that greater skewness and kurtosis parameters substantially amplify tail heaviness and overall dispersion of Y.

9 Comparison of Moments: Exponentiated GC(A) and Exponentiated Zeghdoudi (EZ) distribution

This subsection presents a structural comparison between the moment properties of the exponentiated Gram–Charlier Type A distribution and the exponentiated Zeghdoudi distribution introduced by [8]. Through the comparison, the motivations lies on analytic form, growth behavior, domain of existence and tail implications.

Theorem 9.1. *Let $X \sim GC(A)$ be a standardized Gram–Charlier Type A random variable with cumulants κ_r for $r \geq 3$, and define $Y = e^X$.*

Then for any integer $k \geq 1$, $E(Y^k) = \exp\left(\frac{k^2}{2}\right)\left[1 + \sum_{r\geq 3} \frac{\kappa_r}{r!} k^r\right]$.

In particular, the dominant asymptotic behavior satisfies $E(Y^k) \sim \exp\left(\frac{k^2}{2}\right)$ as $k \to \infty$.

Proof. The moment generating function of X is $M_X(t) = \exp\left(\frac{t^2}{2}\right)\left[1 + \sum_{r\geq 3} \frac{\kappa_r}{r!} t^r\right]$.

Since $Y = e^X$, we have $E(Y^k) = E(e^{kX}) = M_X(k)$.

Substituting $t = k$ yields $E(Y^k) = \exp\left(\frac{k^2}{2}\right)\left[1 + \sum_{r\geq 3} \frac{\kappa_r}{r!} k^r\right]$. For fixed cumulants κ_r, the polynomial term grows at order k^m, whereas the leading exponential term grows at order $e^{k^2/2}$. Hence, $E(Y^k) \sim \exp\left(\frac{k^2}{2}\right)$. □

Theorem 9.2. *Let $Z \sim EZ(c, \theta)$. Then the rth raw moment admits the representation*

$$E(Z^r) = \sum_{j=0}^{\infty} \sum_{i=j}^{\infty} \sum_{k=0}^{j} C_{ijk} \frac{\Gamma(r + \alpha_{ijk})}{[\theta(1+i)]^{r+\alpha_{ijk}}},$$

for suitable constants $C_{ijk}, \alpha_{ijk} > 0$. Moreover, as $r \to \infty$, $E(Z^r) \sim \frac{\Gamma(r+a)}{\theta^r}$ for some constant $a > 0$, and therefore $E(Z^r) \sim \left(\frac{r}{\theta}\right)^r e^{-r}$.

Proof. The triple-series representation follows from the expansion of the EZ density. For large r, the dominant growth is determined by the Gamma function term. Using Stirling's approximation, $\Gamma(r+a) \sim \sqrt{2\pi}\, r^{r+a-1/2} e^{-r}$. Thus, $E(Z^r) \sim \frac{r^{r+a} e^{-r}}{\theta^r} = \left(\frac{r}{\theta}\right)^r e^{-r} r^a$.

Hence, the moment growth is exponential–polynomial rather than quadratic-exponential. □

Proposition 9.3. *Let $Y = e^X$ with $X \sim GC(A)$, and let $Z \sim EZ(c, \theta)$. Then,*

$$\lim_{k\to\infty} \frac{\log E(Y^k)}{k^2} = \frac{1}{2},$$

whereas $\lim_{r\to\infty} \frac{\log E(Z^r)}{r^2} = 0.$

Proof. From Theorem 9.1, we have $\log E(Y^k) = \frac{k^2}{2} + O(\log k)$, which directly implies $\frac{\log E(Y^k)}{k^2} \to \frac{1}{2}$.

On the other hand, using Stirling's approximation for the EZ moments, we get the approximation that $\log E(Z^r) \sim r \log r - r - r \log \theta$. Dividing by r^2, we finally achieve the relation $\dfrac{\log E(Z^r)}{r^2} = \dfrac{r \log r}{r^2} - \dfrac{r}{r^2} - \dfrac{r \log \theta}{r^2} \to 0$, which completes the proof. □

Corollary 9.4. *The* exp{GC(A)} *distribution exhibits quadratic-exponential moment growth, while the EZ distribution exhibits only exponential–polynomial growth. Consequently, high-order sample moments under* exp{GC(A)} *are fundamentally less stable than under the EZ distribution.*

9.1 Growth Rate Analysis

In this subsection we analyze the asymptotic growth behavior of raw moments as $r \to \infty$ and classify the type of divergence exhibited by the EGC(A) and EZ distributions.

9.1.1 (i) Exponentiated Gram–Charlier Type A Distribution

Let $X \sim GC(A)$ be standardized and define $Y = e^X$. The rth raw moment is

$$E(Y^r) = \exp\left(\frac{r^2}{2}\right)\left[1 + \sum_{m\geq 3} \frac{\kappa_m}{m!} r^m\right].$$

For fixed cumulants κ_m, the polynomial term grows at most as $O(r^p)$ for some p. Hence, the dominant term is $E(Y^r) \sim \exp\left(\dfrac{r^2}{2}\right)$. Taking logarithms, we get $\log E(Y^r) \sim \dfrac{r^2}{2}$. Thus, the moment growth is **quadratic-exponential**, i.e., $E(Y^r) = \exp\big(Cr^2\big),\ C = \dfrac{1}{2}$.

9.1.2 (ii) Exponentiated Zeghdoudi Distribution

Let $Z \sim EZ(c, \theta)$. Its rth raw moment admits the asymptotic representation

$$E(Z^r) \sim \frac{\Gamma(r+a)}{\theta^r},$$

for some constant $a > 0$. Using Stirling's approximation, $\Gamma(r+a) \sim \sqrt{2\pi}\, r^{\,r+a-1/2} e^{-r}$. Hence,

$$E(Z^r) \sim \left(\frac{r}{\theta}\right)^r e^{-r} r^a.$$

Taking logarithms, $\log E(Z^r) \sim r \log r - r - r \log \theta$. Thus, we obtain $\log E(Z^r) = O(r \log r)$.

Proposition 9.5. *Let $Y = e^X$ with $X \sim GC(A)$ and $Z \sim EZ(c, \theta)$. Then, one can get,* $\lim\limits_{r\to\infty} \dfrac{\log E(Y^r)}{r^2} = \dfrac{1}{2}$, *whereas* $\lim\limits_{r\to\infty} \dfrac{\log E(Z^r)}{r^2} = 0$.

Proof. From the previous derivation, we have $\log E(Y^r) \sim \frac{r^2}{2}$. Thus, one can conclude that $\frac{\log E(Y^r)}{r^2} \to \frac{1}{2}$.
For the EZ distribution, $\log E(Z^r) \sim r \log r - r - r \log \theta$.
Dividing by r^2, we finally get $\frac{r \log r}{r^2} - \frac{r}{r^2} - \frac{r \log \theta}{r^2} \to 0$. □

Since $\exp\left(\frac{r^2}{2}\right) \gg \left(\frac{r}{\theta}\right)^r e^{-r}$, as $r \to \infty$, we conclude $\lim_{r\to\infty} \frac{E(Y^r)}{E(Z^r)} = \infty$. Thus, the exponentiated Gram–Charlier model diverges strictly faster than the Exponentiated Zeghdoudi model. The $\exp\{GC(A)\}$ distribution exhibits super-exponential (quadratic-exponential) moment divergence, whereas the EZ distribution exhibits controlled polynomial–exponential divergence. This fundamental structural distinction explains the dramatic instability observed in high-order sample moments under Gram–Charlier perturbations.

9.2 Lower-Order Moment Comparison

In this subsection we compare the first four moments of the Exponentiated Gram–Charlier Type A distribution and the Exponentiated Zeghdoudi (EZ) distribution, and analyze their sensitivity to higher-order parameters.

9.2.1 Mean and Variance

(i) Exponentiated Gram–Charlier Type A

Let $X \sim GC(A)$ be standardized and define $Y = e^X$. The first two raw moments are

$$E(Y) = \exp\left(\frac{1}{2}\right)\left[1 + \sum_{m\geq 3} \frac{\kappa_m}{m!}\right], \quad E(Y^2) = \exp(2)\left[1 + \sum_{m\geq 3} \frac{\kappa_m}{m!} 2^m\right].$$

that follows $\mathrm{Var}(Y) = E(Y^2) - (E(Y))^2$. Even moderate values of κ_3 or κ_4 amplify $E(Y^2)$ through the factor 2^m, producing rapid variance inflation.

(ii) Exponentiated Zeghdoudi Distribution

For $Z \sim EZ(c, \theta)$, the first two raw moments can be expressed using a gamma-type expansion, giving $E(Z) = \mu_1'$ and $E(Z^2) = \mu_2'$. Both quantities are finite combinations of Gamma functions scaled by powers of θ. Consequently, the variance takes the form $\mathrm{Var}(Z) = \mu_2' - (\mu_1')^2$, and its dominant behavior is of order $O(\theta^{-2})$.

9.2.2 Coefficient of Variation

The coefficient of variation (CV) is $\mathrm{CV} = \frac{\sqrt{\mathrm{Var}(X)}}{E(X)}$. For $Y \sim \exp\{GC(A)\}$, one can obtain $\mathrm{CV}(Y) = \sqrt{\frac{\exp(2)\left[1 + O(\kappa_m 2^m)\right]}{\exp(1)\left[1 + O(\kappa_m)\right]^2} - 1}$. Thus, CV grows rapidly with higher-order

cumulants. For EZ, $\mathrm{CV}(Z) = \dfrac{\sqrt{\mu_2' - (\mu_1')^2}}{\mu_1'}$, which remains bounded provided $\theta > 0$.

9.2.3 Skewness and Kurtosis

(a) Exponentiated GC(A)

Since $Y = e^X$, higher standardized moments involve $E(Y^3) = \exp\left(\frac{9}{2}\right)\left[1 + \sum_{m\geq 3} \frac{\kappa_m}{m!} 3^m\right]$.

Thus skewness and kurtosis contain terms proportional to $\exp(9/2)$ and $\exp(8)$, respectively. Hence even moderate κ_3, κ_4 produce explosive tail amplification.

(b) Exponentiated Zeghdoudi

Skewness and kurtosis are smooth functions of (c, θ) through Gamma expressions. No quadratic-exponential amplification occurs.

(c) Sensitivity to Higher-Order Parameters

For $\exp\{GC(A)\}$: $\dfrac{\partial E(Y^r)}{\partial \kappa_m} = \dfrac{r^m}{m!} \exp\left(\dfrac{r^2}{2}\right)$. Hence sensitivity grows as $r^m e^{r^2/2}$.

For EZ, sensitivity is of order $O\left(\dfrac{\Gamma(r+a)}{\theta^r}\right)$, which is significantly slower.

9.3 Moment Existence and Stability

We now examine moment existence, convergence properties, and potential moment explosion.

9.3.1 Moment Generating Function and Radius of Convergence

(A) Exponentiated GC(A)

The moment generating function of X is $M_X(t) = \exp\left(\frac{t^2}{2}\right)\left[1 + \sum_{m\geq 3} \frac{\kappa_m}{m!} t^m\right]$. Since $\exp(t^2/2)$ is entire, $M_X(t)$ is analytic for all $t \in \mathbb{R}$. Therefore, $E(Y^r) = M_X(r)$ exists for all finite r. However, $\lim_{r\to\infty} E(Y^r) = \infty$ with super-exponential divergence.

(B) Exponentiated Zeghdoudi

For $Z \sim EZ(c, \theta)$, the density behaves as $z(1+z)e^{-\theta z}$. Hence, for $\theta > 0$,

$$\int_0^\infty z^r e^{-\theta z} dz < \infty \quad \forall r > 0.$$

Thus all positive moments exist provided $\theta > 0$.

9.3.2 Moment Explosion

In simple terms, moment explosion describes a situation where the moments $E(X^r)$ grow extremely fast as the order r increases—so fast that their growth rate exceeds even that of an exponential function. For this model based on $\exp\{GC(A)\}$, the growth of moments follows the pattern $E(Y^r) \sim \exp\left(\frac{r^2}{2}\right)$, which increases much faster than a standard exponential rate. Consequently, $\lim_{r\to\infty} \frac{\log E(Y^r)}{r} = \infty$, indicating a super-exponential explosion of moments. This highlights the extremely heavy upper-tail behaviour of the distribution.

(C) EZ Distribution

For the EZ distribution, the growth of moments is comparatively more controlled. In particular, $\log E(Z^r) \sim r \log r$, which still diverges as $r \to \infty$, since $\lim_{r\to\infty} \frac{\log E(Z^r)}{r} = \infty$, but at a much slower rate than in the previous case. This is further clarified by $\frac{\log E(Z^r)}{r^2} \to 0$, showing that the growth is sub-quadratic in comparison.

Thus, while both models admit all positive moments, their behavior is fundamentally different. The $\exp\{GC(A)\}$ model exhibits a much more aggressive, quadratic-exponential type of moment explosion, whereas the EZ distribution shows a more tempered, parameter-controlled growth. This difference helps explain why high-order moment estimation tends to be far more unstable under Gram–Charlier type perturbations than under the EZ framework.

9.4 Tail Implications

We now relate the asymptotic moment growth behavior to right-tail heaviness and extreme-value modeling implications.

9.4.1 Right-Tail Behavior of $\exp\{GC(A)\}$

Let $X \sim GC(A)$ be standardized and define $Y = e^X$. The density of Y is

$$f_Y(y) = \frac{1}{y}\phi(\log y)\left[1 + \sum_{m\geq 3} \frac{\kappa_m}{m!} H_m(\log y)\right], \quad y > 0.$$

Since $\phi(\log y) = \frac{1}{\sqrt{2\pi}} \exp\left(-\frac{(\log y)^2}{2}\right)$, then $f_Y(y) \asymp \frac{1}{y} \exp\left(-\frac{(\log y)^2}{2}\right)$ as $y \to \infty$. Thus, the right tail satisfies $\log f_Y(y) \sim -\frac{(\log y)^2}{2}$.

9.4.2 Right-Tail Behavior of EZ Distribution

For $Z \sim EZ(c, \theta)$, the density behaves as $f_Z(z) \asymp z(1+z)e^{-\theta z}, \quad z \to \infty$.
Hence, $\log f_Z(z) \sim -\theta z$. Thus, the EZ distribution belongs to the light-tailed class.

9.4.3 Moment Growth and Tail Heaviness

A common concept in probability theory is that if the moments of a distribution increase very rapidly, then that distribution is said to be heavy-tailed. The present context is as follows. The moments of Y are extremely rapid and take an approximate form as $E(Y^r) \sim \exp\left(\frac{r^2}{2}\right)$. The moments of Z grow much more slowly and take an approximate form as $E(Z^r) \sim \left(\frac{r}{\theta}\right)^r e^{-r}$. As a result, we arrive at an important conclusion: the $\exp\{GC(A)\}$ model has a much heavier effective right tail compared to the EZ distribution.

9.4.4 Extreme-Value Modeling Implications

The Exponentiated GC(A) distribution can generate very large upper-tailed values and thus is well-suited for modeling extremely dangerous or volatile risks. While it offers this flexibility, the distribution puts a cost on higher sample moments by making the sample moments unstable, leading the model to be overly sensitive to changes in skewness and kurtosis.

On the other hand, behavior of tails in the Exponentiated Zeghdoudi distribution is controlled by the parameter θ. This makes the distribution function stable and makes the distribution function very applicable for the field of reliability and survival analysis. Additionally, it tends to be much more useful for moderate extreme values.

The quadratic-exponential moment growth of $\exp\{GC(A)\}$ grows more quickly than the tail of the EZ distribution which decreases exponentially. This difference in the tail structure affects the modeling of high-risk data and extreme-value data.

10 Conclusion

Using the standard Gram–Charlier Type A distribution, one can systematically move beyond the traditional Gaussian setup through incorporation of the statistical properties namely skewness, kurtosis, higher deviations through cumulants etc. The analytical form of the distribution is explained through the characteristic function, cumulant generating function, relationships among various order moments, etc. Particularly, the characteristic function is derived as $\varphi(t) = e^{-t^2/2}\left[1 + \sum_{r=3}^{\infty} \frac{\kappa_r}{r!}(it)^r\right]$ that is clearly different from that of the Gaussian distribution using higher-order corrections. The cumulant generating function $K(t) = \frac{t^2}{2} + \sum_{r=3}^{\infty} \frac{\kappa_r}{r!} t^r$ explains the deviations from normality with the aid of cumulant based terms. For lower order raw moments these cumulants are translated into explicit expressions as $\mu_3 = \kappa_3$, $\mu_4 = 3 + \kappa_4$, and $\mu_6 = 15 + 15\kappa_4 + 10\kappa_3^2$. A clear pattern is followed henceforth; skewness exhibits linearity, kurtosis is an addition to the Gaussian framework, more complex interactions are explained by higher order moments including nonlinear effects (e.g. by κ_3^2). As a result, the propagation of asymmetry and tail behaviour is observed in a reasonable way.

Furthermore, the model is exponentiated as a natural extension as follows; if $X \sim \mathrm{GC(A)}$ and $Y = \exp(X)$ then the resulting probability distribution enters into multiplicative setup, with support restricted to $(0, \infty)$ which enable modelling for strictly positive data. Y has the moment structure $E(Y^r) = \exp\left(\frac{r^2}{2} + \sum_{k=3}^{\infty} \frac{\kappa_k}{k!} r^k\right)$, which is directly determined from the cumulant generating function. From this expression, it can be observed that higher order cumulants grow via exponential amplification, and if all higher-order cumulants are approximately 0 then this model gets reduced to classical lognormal distribution. Nonzero cumulants control the deviations in tail thickness and asymmetry for flexible modelling of positive data with heavy tails.

In summary, the Gram-Charlier Type A distribution and its exponentiated version together provide a consolidated, analytically convenient system for studying non-Gaussian behavior. The cumulant-based formulation used here provides both structural clarity and explicit moment. The formulation is flexible and provides both additive and multiplicative modeling features. Consequently, this formulation is valuable for use in advanced statistical models, such as asymptotic and tail models, semiparametric models, and situations when the normal and lognormal models are excessively constraining.

Acknowledgement

The authors thank each other for developing this insightful work.

Competing Interests

The authors agree that no potential conflict of interest exists for this work.

Funding

No funding is applicable for this research work.

Ethics Statement

In this study, human participants as well as animals have not been used.

References

[1] Bhattacharya, R. N. and Rao, R. R. (1976). *Normal Approximation and Asymptotic Expansions*. Wiley.

[2] Charlier, C. V. L. (1905). Über die darstellung willkürlicher funktionen. *Arkiv för Matematik, Astronomi och Fysik*, 2:1–20.

[3] Charlier, C. V. L. (1906). Über die darstellung willkürlicher funktionen ii. *Arkiv för Matematik, Astronomi och Fysik*, 3:1–34.

[4] Cramér, H. (1946). *Mathematical Methods of Statistics*. Princeton University Press.

[5] Gram, J. P. (1883). Ueber die entwicklung reeller funktionen in reihen mittels der methode der kleinsten quadrate. *Journal für die reine und angewandte Mathematik*, 94:41–73.

[6] Kendall, M. and Stuart, A. (1977). *The Advanced Theory of Statistics, Vol. 1*. Charles Griffin.

[7] Ruidas, M. K. (2020). Transmuted zeghdoudi distribution: Theory and applications. *Int. J. Sci. Res. in Mathematical and Statistical Sciences Vol*, 7(2):95–101.

[8] Ruidas, M. K., Khan, M., Das, S., and Alzoubi, L. M. (2025). The exponentiated zeghdoudi distribution: properties, simulations, regression, and applications. *Life Cycle Reliability and Safety Engineering*, pages 1–14.